Muon Energy Loss Upstream of the Muon Spectrometer

K. Nikolopoulos, D. Fassouliotis, C. Kourkoumelis*
University of Athens
A. Poppleton
CERN

January 17, 2007

Abstract

A method for the estimation of the muon energy loss upstream of the Muons Spectrometer is presented. The method provides an improved and updated parametrization of the muon energy loss in ATLAS, along with an estimation based on the actual energy deposition in the calorimeters. The latter aims to account, on an event-by-event basis, for the statistical fluctuations of the energy loss.

The final implementation of the presented method combines both the energy loss parametrization and the calorimeter information. This Hybrid method provides on the average a 5% improvement on the muon stand-alone momentum resolution, reaching 10% for $P_T = 100 GeV/c$, and reduces the non-Gaussian tails. The method is implemented inside the ATHENA framework, in the MuidCaloEnergyTools package.

*Corresponding author: Christine.Kourkoumelis@cern.ch

1 Introduction

The tasks of muon identification and momentum measurement in the ATLAS experiment can be performed using the Muon Spectrometer (MS) alone (Stand-alone muon reconstruction). However, in order to improve the resolution on the measurement of the muon momenta, the information provided by the Inner Detector (ID) is combined with the one provided by the MS (Combined muon reconstruction).

In the low momentum region, the precision of the momentum measurement is determined by the accuracy of the ID, and the MS is used only to provide the muon identification. At higher momenta, the MS provides most of the information in the momentum measurement. The crossover point spans from $P_T = 80\,GeV/c$ in the barrel to $P_T = 20\,GeV/c$ in the forward region (Figure 1).

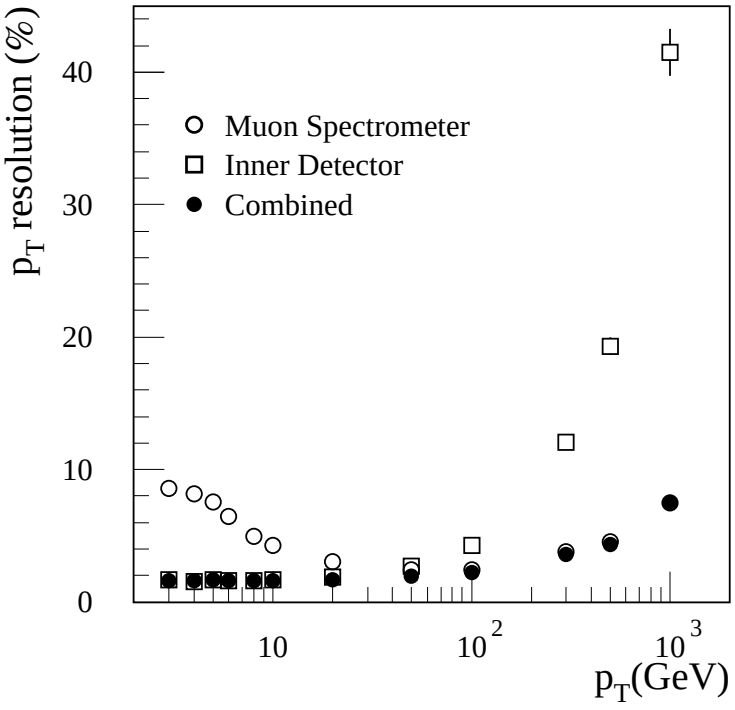

Figure 1: The resolution of the muon momentum measurement from the MS, the ID and their combination, averaged over pseudorapidity, as a function of P_T. [1]

In both momentum regions the estimation of the energy loss of the muon upstream of the MS is essential. In the high P_T region, it has to be added to the momentum determined by the stand-alone MS in order to estimate the P_T of the muon at the interaction point (IP). In the low P_T region, accurate knowledge of muon energy loss facilitates the matching between the ID and MS tracks and results in a better combined measurement.

The energy loss by the muons in matter, for momenta below approximately $200\,GeV/c$ [2], is described by the Bethe-Block formula for the dE/dx ionization losses and roughly follows a Landau distribution. At higher momenta, the energy loss due to radiation effects

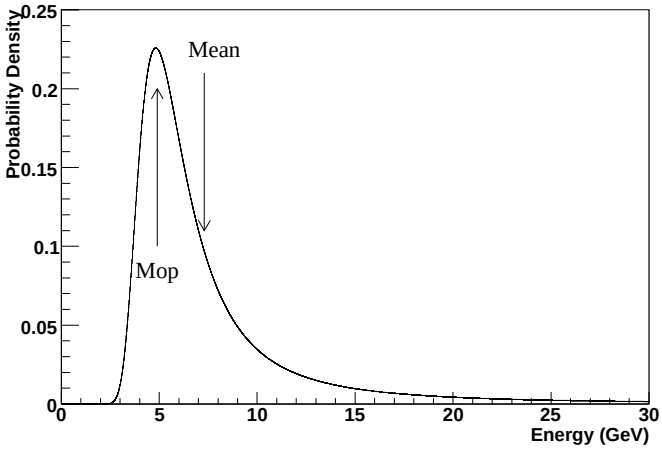

Figure 2: A Landau distribution of the energy loss with $mop = 5\,GeV$ and $\sigma = 0.8\,GeV$. The mean and the most probable (mop) energy loss values are indicated.

is equally important as the ionization and should be accordingly taken into account.

In order to account for the energy loss when extrapolating a muon from the MS to the IP, one has to add either the most probable energy loss (mop) or the mean value of the energy loss (Figure 2). These energy loss estimations are statistical quantities which can not take into account the event-by-event energy loss fluctuations. However, the former seems more appropriate, since it gives a better description of the energy loss for the majority of the muons, especially for momenta below $200\,GeV/c$. The muon energy loss estimation used in the ATLAS software up to ATHENA release 10.3.0 was a parametrization of the mean energy loss as a function of the momentum measured in the MS and the amount of the traversed material.

In this note, a more accurate energy loss parametrization is described both for the mean and the mop energy loss, having asymmetric errors. In addition, a method using the calorimeter information needed to account for the energy loss fluctuations on an event-by-event basis is presented. The present study is performed using one of the two muon reconstruction algorithms available, namely the Moore/Muid [3], but it can be applied to the Muonboy [4] as well.

In Section 2 of this note, the updated energy loss parametrization and its validation is presented along with a comparison to the previous one. In Section 3 the method exploiting the calorimetric measurement is presented in detail, while in Section 4 the necessary muon isolation criteria for its application are established. The performance of the introduced method based on single muon events is discussed in detail in Section 5. In Section 6, the effects of the pile-up and the cavern background on the energy loss measurement are discussed and finally in Section 7 the conclusions of this study are presented.

In all the following sections the term "resolution" will be used to denote, according to the context, either the distribution of the difference between the estimation of a quantity

and the corresponding true value or the Gaussian standard deviation, σ, of this distribution. In addition, the term "relative" will be used when the difference is divided with the true value.

The term "momentum scale" is defined as the Gaussian mean of the relative momentum resolution distribution, while the shorthands "Moore","Muid StandAlone" and "Muid Combined" will denote the muon track parameters as reconstructed at the MS entrance, as extrapolated at the point of closest approach to the IP and when combined with the corresponding ID track, respectively.

Finally, the following values for the muon energy loss upstream the MS will be used

- E_{Loss}^{True} the Monte–Carlo simulated muon energy loss upstream the MS.
- E_{Loss}^{Mop} the muon energy estimated by the *Mop* parametrization.
- E_{Loss}^{Mean} the muon energy loss estimated by the *Mean* parametrization.
- E_{Loss}^{Meas} the muon energy loss estimated using the calorimeter measurement only.
- $E_{Loss}^{Hybrid} \equiv E_{Loss}^{Meas/Mop}$ the muon energy loss estimated using the combination of the calorimeter measurement and the *Mop* parametrization.

Moreover, the symbols $\sigma_{Mop}, \sigma_{Hybrid} \equiv \sigma_{Meas/Mop}$ will denote the resolutions of the corresponding energy loss estimation methods.

2 The new energy loss parametrization

The previous parametrization of the energy loss (ATHENA release $< 10.4.0$) as a function of the momentum and pseudorapidity (η) was based on a set of constant P_T single muon samples. Only the "mean" of the distribution was parametrized, using a third degree polynomial. A symmetric uncertainty was assigned to the estimated energy loss values, based on the parametrization of the RMS of the distributions.

In order to derive the present "new" parametrization, eight constant P single muon samples in the range $5 - 1000\ GeV/c$ were used to parametrize both the "mean" and the "mop". The significant increase of statistics - each sample contained 10^4 events - with respect to the previous parametrization, permitted the division of the sample in finer pseudorapidity bins ($\Delta\eta = 0.1$). Each sample was simulated, digitized and reconstructed with ATHENA release 10.0.1.

As mentioned above, the mop value describes better the majority of the muons and is therefore used as the default energy loss parametrization since ATHENA release 10.4.0. In this section, the results on the mean value are presented as well, in order to compare with the previous parametrization.

The mop and the mean energy loss for each momentum was computed using roughly 700 muons per η bin. In Figure 3 the True energy loss distributions for four values of momentum are presented for the η bin 0.4-0.5. The mean energy loss was estimated using

the mean of the distribution in each (η, P) bin, while the mop value was derived by a Landau fit. Next, the energy loss was parametrized using a continuous three parameter function of momentum which exploits the physical aspects of the energy loss:

$$E_{Loss}^{Par} = a_0 + a_1 ln(A \cdot P^2) + a_2 \cdot P \tag{1}$$

The first term on this function describes the minimum ionizing part of the muon energy loss, while the second and the third terms describe the relativistic rise and the radiative effects respectively. Note that the parameter

$$A = 0.0067\ (GeV/c)^{-2}$$

which describes the relativistic rise was kept constant for all η bins.

Then, a fit as function of momentum was performed in all η bins estimating the free parameters of the above formula. This η binning essentially accounts for the different amount of material traversed by the muon in each case. Furthermore, the parametrization

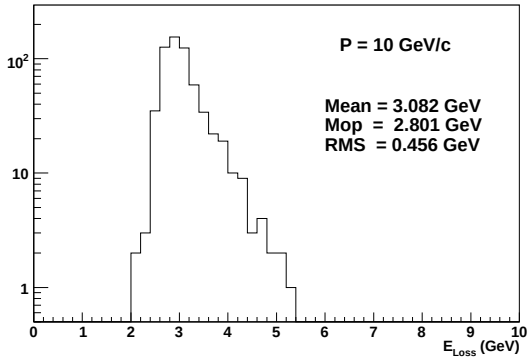

(a) $10\ GeV/c$

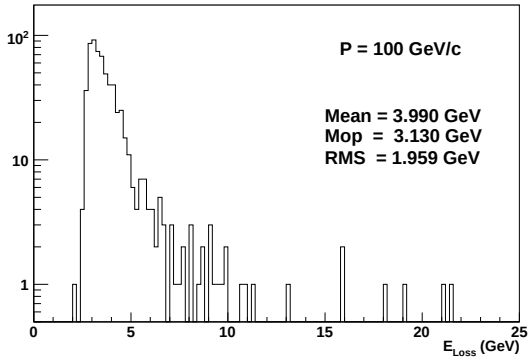

(b) $100\ GeV/c$

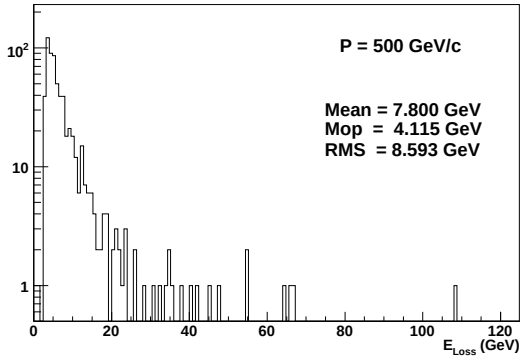

(c) $500\ GeV/c$

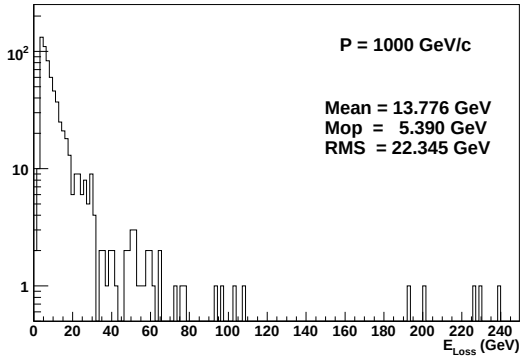

(d) $1000\ GeV/c$

Figure 3: The True muon energy loss (E_{Loss}^{True}) distribution for the η interval 0.4-0.5 and four different momentum values.

was calculated using the true momenta of the muons at the entrance of the MS, decoupling the energy loss estimation from the performance of the stand-alone MS reconstruction.

In both cases (mop and mean), the errors on the parametrized values were estimated by measuring the 90% probability intervals in each set of muons separately from the left and right side of the distributions. These widths were then transformed into normal asymmetric standard deviations, which provide a more realistic estimation of the energy loss fluctuations. At the same time, the width, σ_{Landau}, of the Landau distribution has been parametrized. In Figure 4 an example of the *Mop* parametrization for the η bin 0.4-0.5 is shown together with its σ_{Landau}.

In order to validate the new parametrization, the estimated parametrized energy loss, E_{Loss}^{Par}, was compared to the True energy loss, E_{Loss}^{True}, given by the Monte Carlo. Nine independent single muon samples of constant P_T in the range of $10 - 1000\,GeV/c$ were used for this purpose (Appendix A).

Figure 5(a) shows the mean difference between the energy loss estimated using the old/new *Mean* parametrization and the True energy loss, normalized to the mean True energy loss, as a function of the P_T. Clearly, the new parametrization describes much better the energy loss for momenta above $50\,GeV/c$. The same quantity for the *Mop* parametrization is also shown. As expected, since the comparison is based on the mean values of the distributions, the *Mop* parametrization fails at large momenta, where the radiation effects are important. Nevertheless, as it is shown in Figure 5(b), the Gaussian mean values of the difference between the *Mop* parametrization and the True energy loss, normalized to the mean True energy loss, are consistent with zero for the whole momentum range from $10 GeV/c$ up to $1000 GeV/c$ as expected. Figure 5(c) presents the same comparison between parametrizations but this time using the RMS of the distributions. These RMS values increase with increasing P_T of the muon due to the large negative tails of the $E_{Loss}^{Par} - E_{Loss}^{True}$ distribution. They are independent of the parametrization used and only depend on the actual energy loss of each muon. In Section 3, a strategy is presented which uses the calo-

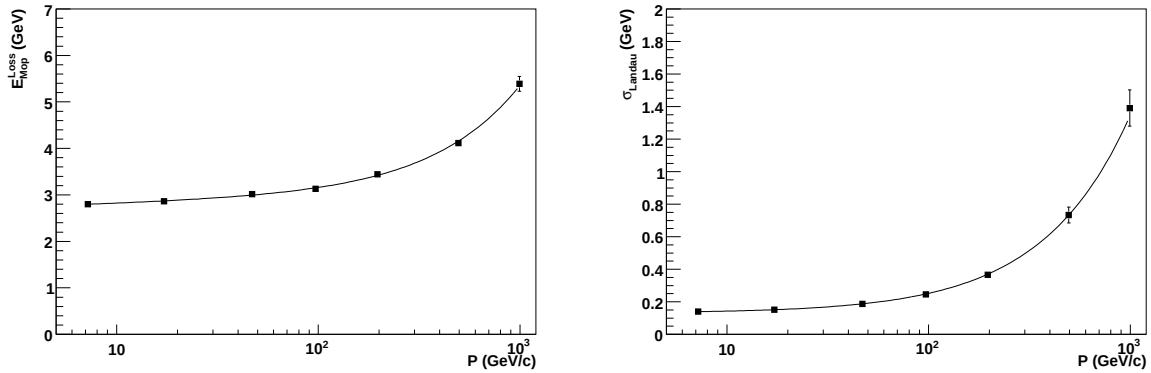

(a) Mop energy loss

(b) Landau width of the energy loss distribution

Figure 4: Example of the *Mop* parametrization and its Landau width (σ_{Landau}) for $0.4 < |\eta| < 0.5$.

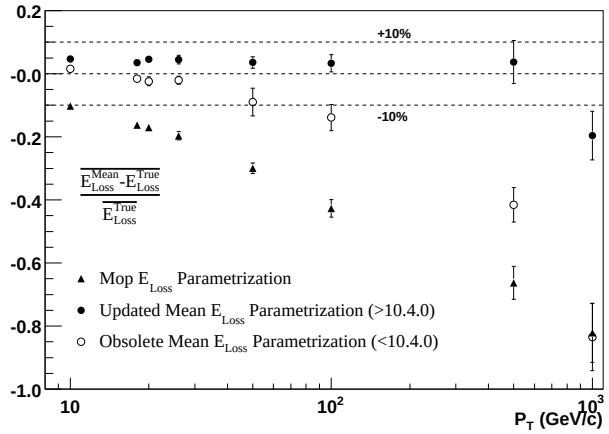

(a) The mean of $(E_{Loss}^{Par} - E_{Loss}^{True})/\overline{E_{Loss}^{True}}$.

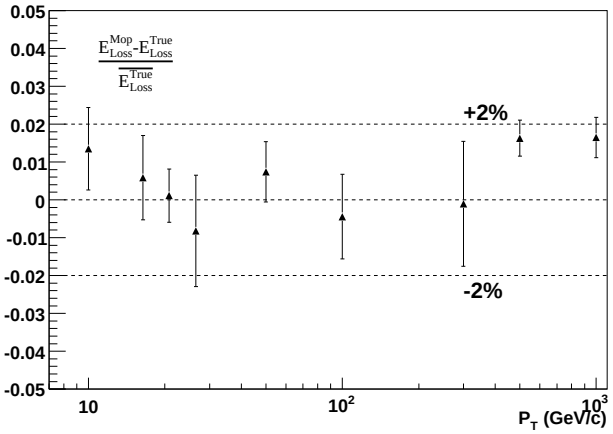

(b) The Gaussian mean of $(E_{Loss}^{Mop} - E_{Loss}^{True})/\overline{E_{Loss}^{True}}$.

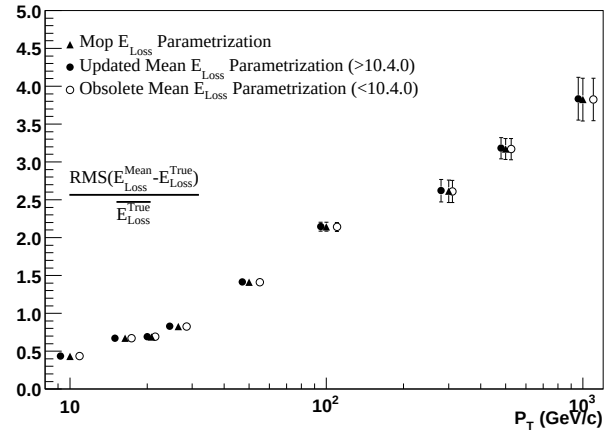

(c) The RMS of $(E_{Loss}^{Par} - E_{Loss}^{True})/\overline{E_{Loss}^{True}}$.

Figure 5: Performance of the three parametrizations described in the text as a function of P_T.

rimeter information on the muon energy deposition in order to reduce this dispersion.

The new energy loss parametrizations are a part of the official ATLAS software, implemented within the MuidCaloEnergyTools package, and are a part of ATHENA since release 10.4.0[1].

2.1 Improvements in the *Mop* parametrization of the energy loss

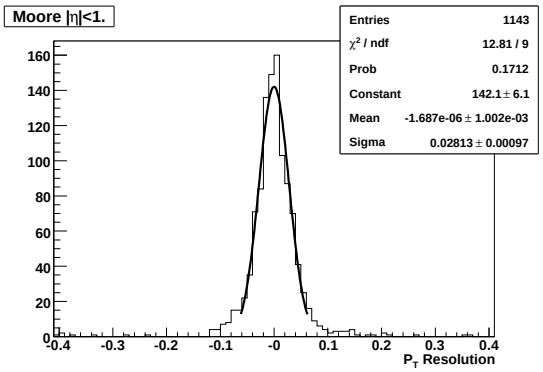

(a) At the entrance of the MS (Moore).

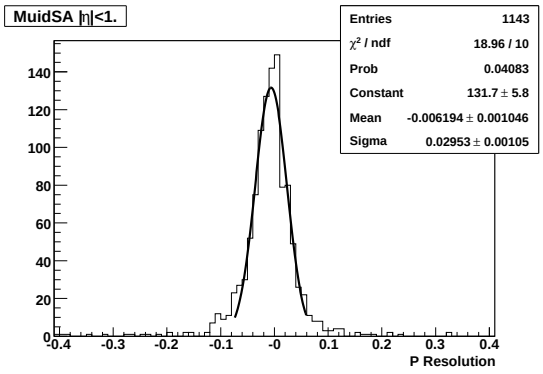

(b) At the IP (Muid Stand-alone) using the mop without any correction.

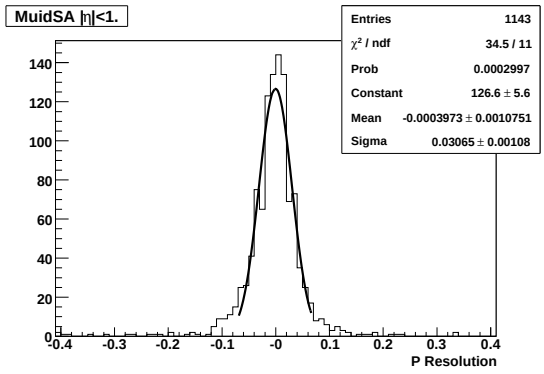

(c) At the IP (Muid Stand-alone) using the mop with the correction described in Appendix B.2.

Figure 6: Relative momentum resolution for single muons of $P_T = 100\,GeV/c$ and $|\eta| < 1$.

As explained in Appendix B.1 using a toy Monte - Carlo, in order to obtain the momentum at the IP one cannot simply add the *Mop* parametrized value to the muon momentum measured in the MS, since a shift in the muon momentum is introduced due to the convolution of the Gaussian uncertainty on the momentum measurement in the MS and the asymmetric Landau distribution of the energy loss of the muons. The result of the shift is the systematic underestimation of the thus estimated momentum at the IP.

[1]The choice between the *Mean* and the *Mop* parametrization is handled by a flag in the jobOptions file. The default and strongly recommended choice is the latter.

In order to account for this effect, the correction described in Appendix B.2 is applied. The influence of the correction on the *Mop* parametrization is illustrated in Figure 6 where the correction was applied on a muon sample of $P_T = 100\,GeV/c$. The shift on the relative momentum resolution, which is small but statistically significant in Figure 6(b) practically disappears in Figure 6(c) after the correction is applied.

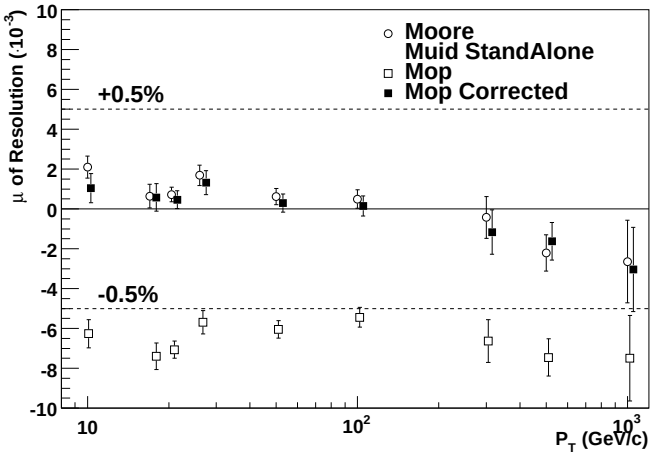

Figure 7: Gaussian mean (μ) of the relative momentum resolution as a function of the P_T.

The effect of the correction on the Gaussian mean of the relative momentum resolution over a wide range of P_T is presented in Figure 7. It can be clearly seen that the correction successfully restores the mean to the nominal value.

3 Estimation of the muon energy loss using the calorimeters / Description of the Hybrid method

A muon traversing the calorimeters looses energy, which in most cases is well described by the *Mop* parametrization of Section 2. Nevertheless, there are cases where the muon suffers a larger energy loss lying on the Landau tail, where the True Energy Loss is significantly larger than the mop energy loss. An effort to extract information of the muon energy loss on an event-by-event basis has been undertaken, in order to reduce the spread of the tails by recovering these events, and in order to improve the overall resolutions.

The only part of the ATLAS detector which is able to provide an event-by-event information on the muon energy loss is the calorimetry. In addition, the ATLAS calorimeters account for more than 80% of the material traversed by the muons upstream of the MS (Section 3.4). Thus, it is expected that most of the energy loss fluctuations will occur inside the calorimeters. As a result, the calorimetric measurement of the muon energy deposition was exploited in order to account for the energy loss fluctuations.

The use of the measured energy in the calorimeters is reasonable only for the case of isolated muons where the measured energy reflects the energy deposited by the muon in question only. Moreover, the estimation and subtraction of the calorimeter noise is of equal importance. These possible sources of deterioration of the energy loss estimation were studied (Section 3.3, Section 4 and Section 6) during the devolpment of this method.

3.1 Measurement of the muon energy loss in the calorimeters

In order to estimate the calorimetric energy loss of each muon, the energy deposition in a cone around the muon track in each calorimeter traversed had to be estimated. Each muon track is extrapolated back to the calorimeter using the "CaloScattering" Model [3].

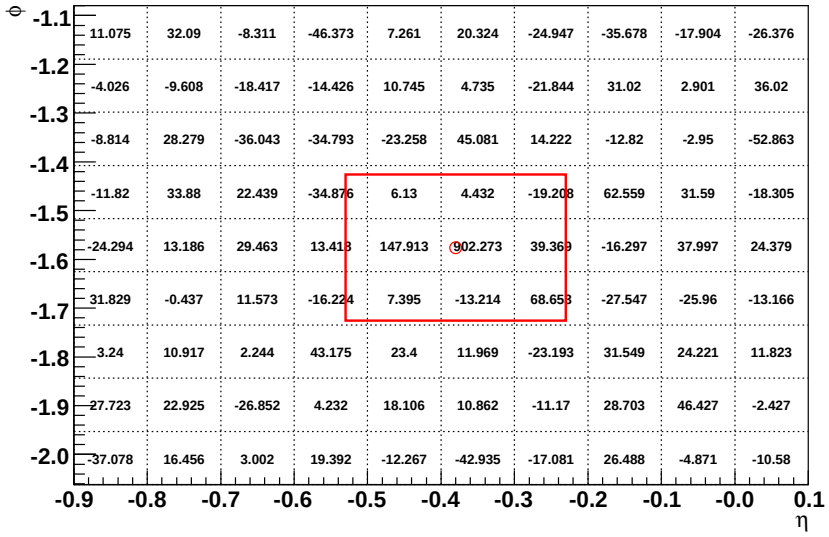

Figure 8: A Tile Calorimeter sampling of a typical muon track expanded in the (η, ϕ) plane. The energy recorded in each cell (in MeV) is shown, along with the muon track (red circle) and the measurement area (red square). Note that the maximum energy deposition coincides with the cell traversed by the muon.

Cones of radius R (Figure 8) were formed[2] for each calorimeter traversed by the muon (The cone sizes are described in Section 3.2). Within each cone, the cells with recorded energy $E_{Cell} > 4 \cdot \sigma_{noise}$ are added. This is the noise suppresion scheme used, a global asymmetric cell level cut. The noise level σ_{noise}, which is actually the RMS of the noise distribution at cell level, is given by the standard Calorimeter tool ("CaloNoiseTool"). Special attention has to be paid for the cases where the signal is of the same order of magnitude as the noise, as discussed in detail in Appendix E.

[2] $R = \sqrt{(\Delta\eta)^2 + (\Delta\phi)^2}$

The energy depositions in the electromagnetic and the hadronic parts are added in order to form the total measured energy deposition upstream of the MS. Furthermore, the measured energy is corrected for the $\frac{e}{mip}$ ratio, since the calorimeter measurement is calibrated to the electromagnetic energy scale [5]. Besides the calorimetric energy, one has to take into account the energy deposited in the additional material traversed by the muon (e.g. the cryostats). This inert or "dead" material is given in radiation lengths by the material map of Section 3.4. The resulting energy is defined as the "Measured" energy loss (E_{Loss}^{Meas}).

Subsequently, the muons are classified into two categories according to their measured energy loss. In the case where the E_{Loss}^{Meas} exceeds the $E_{transition} = mop + 2 \cdot \sigma_{Landau}$, these muons are considered as suffering a large energy deposition[3] (Category 1) and the E_{Loss}^{Meas} is used to estimate their energy loss. However, if the "Measured" energy does not exceed the $E_{transition}$ then the *Mop* estimation is used for the muon energy loss (Category 2). This classification into two categories is a result of the fact that the calorimeters perform more accurate measurements in the case of large energy depositions, while the *Mop* parametrization offers an accurate description of the small energy depositions.

It is important to note that, given the distribution of the energy loss, the majority of the muon tracks belong to the second category (Figure 9). On the other hand, the energy loss determination using the E_{Loss}^{Meas} for the fraction of muons with large energy deposition provides an estimate which is much closer to the True energy loss, as will

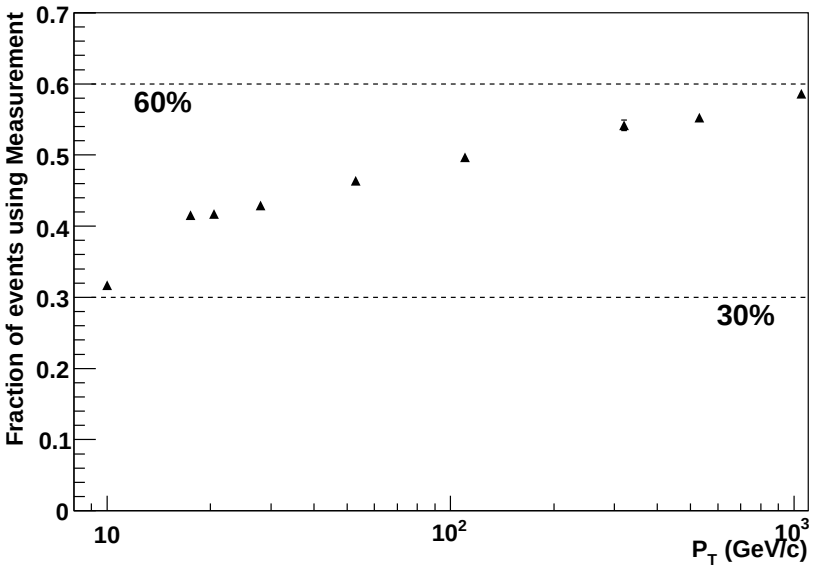

Figure 9: Fraction of events suffering large energy loss (Category 1) as a function of P_T.

be shown later. The final estimation of the muon energy loss is a combination of the

[3]The specific choice of $E_{transition}$ is explained in Appendix C.

calorimeter measurement and the *Mop* parametrization, and this method will be called the "Hybrid Meas/Mop" method hereafter[4].

3.2 Cone size study

In order to calculate the energy deposition, the energy of the cells within a cone around the muon track has to be added. There are two competing effects which should be taken into account for the definition of the cone width. A large cone would add more background to the energy measurement, while a small one could result in underestimation of the energy deposition. Therefore, the cone size should be optimized with respect to the extrapolation uncertainty of the muon track from the MS to the calorimeters and the noise added to the measurement.

A study of different cone sizes was performed. The optimum values were found to be $R = 0.15$ for the Tile and the LArHEC and $R = 0.075$ for the LArEM. Figure 10 shows that using larger cones does not improve the measurement of the energy deposition and hence the energy resolution. On the other hand, narrower cones would lead to certain loss of information, because the used cone sizes are already of the order of a cell width in the hadronic calorimeters and consistent with the muon extrapolation uncertainty in the electromagnetic calorimeter.

3.3 Noise study

The muon energy deposition in the calorimeters is low when compared to the energy deposited by the physics objects (jets, electrons, photons, etc.) which the ATLAS calorimeters are designed to measure. Actually, signals from muons are often used in calorimetry to test and validate the quality of the detector's performance in the low energy regime.

An important consideration for the measurement of the muon energy deposition is the noise at the cell level. The origin of this noise can either be electronics or physics (pile-up). In the case where the muon signal is overwhelmed by the noise of the cell, it is obvious that no measurement can be performed. Therefore, the primary concern is the comparison of the noise levels in the ATLAS calorimeters with the expected muon signals and the decision of whether the S/N ratio is significantly larger than one.

In Appendix D, detailed tables and figures are given with the expected mean and sigma of the noise for each sampling and for two different pile-up conditions. In Figure 11 the expected muon signal and noise for the 3^{rd} sampling of the Tile Calorimeter are compared. The expected signal is well above the noise distribution with $S/N \approx 23$. The electronic noise levels in the ATLAS calorimeters are of $O(20MeV)$ for Tile and LArEM and of $O(200MeV)$ for the LArHEC.

From the presented noise levels in the ATLAS calorimeters, it can be concluded that it is possible to perform measurements down to very small energy depositions in the central

[4]The shorthands "Hybrid" method and "Meas/Mop" method will also refer to the same method.

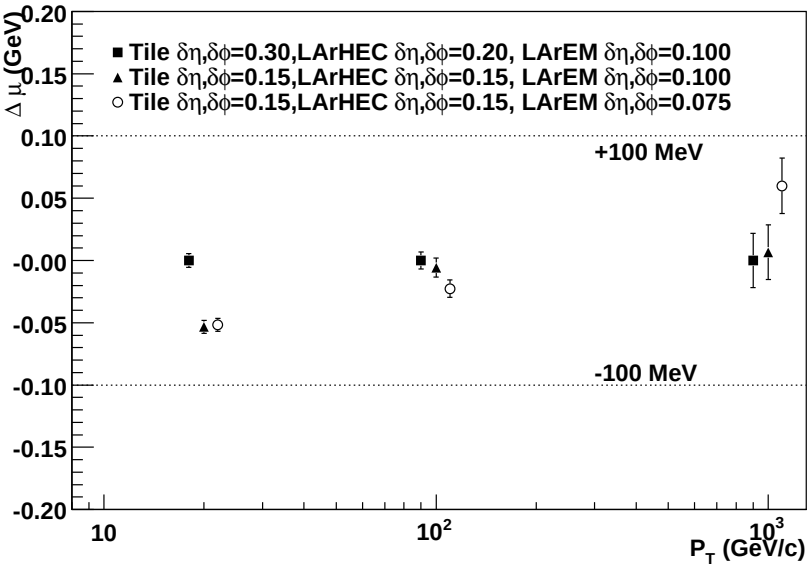

(a) The Gaussian mean (μ) of the ($E_{Loss}^{Meas} - E_{Loss}^{True}$) as a function of P_T for different cone sizes. The results are expressed as differences with respect to the case with $(\delta\eta, \delta\phi)_{Tile} = 0.3$,$(\delta\eta, \delta\phi)_{LArHEC} = 0.2$,$(\delta\eta, \delta\phi)_{LArEM} = 0.1$

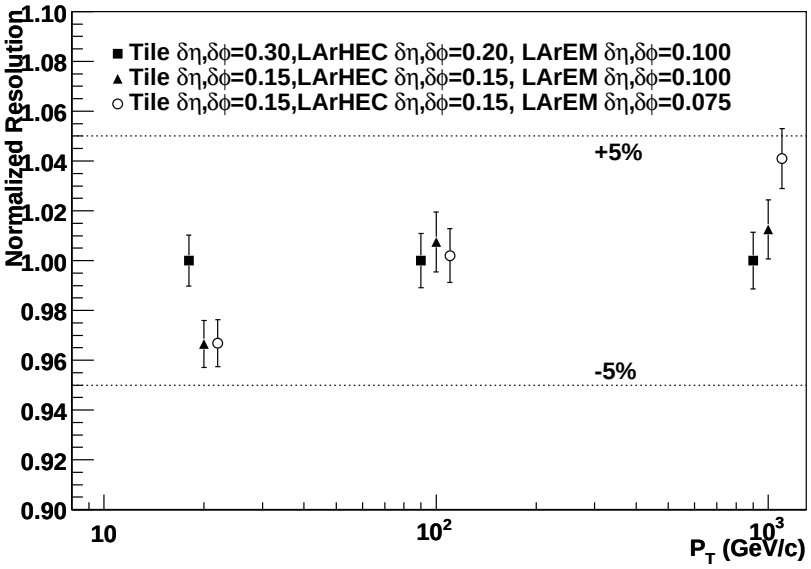

(b) The Gaussian standard deviation σ of the ($E_{Loss}^{Meas} - E_{Loss}^{True}$) as a function of P_T for different cone sizes. The results are normalized to the σ of the case with $(\delta\eta, \delta\phi)_{Tile} = 0.3$,$(\delta\eta, \delta\phi)_{LArHEC} = 0.2$,$(\delta\eta, \delta\phi)_{LArEM} = 0.1$

Figure 10: Gaussian mean and standard deviation of $E_{Loss}^{Meas} - E_{Loss}^{True}$ as a function of the P_T for different cone sizes.

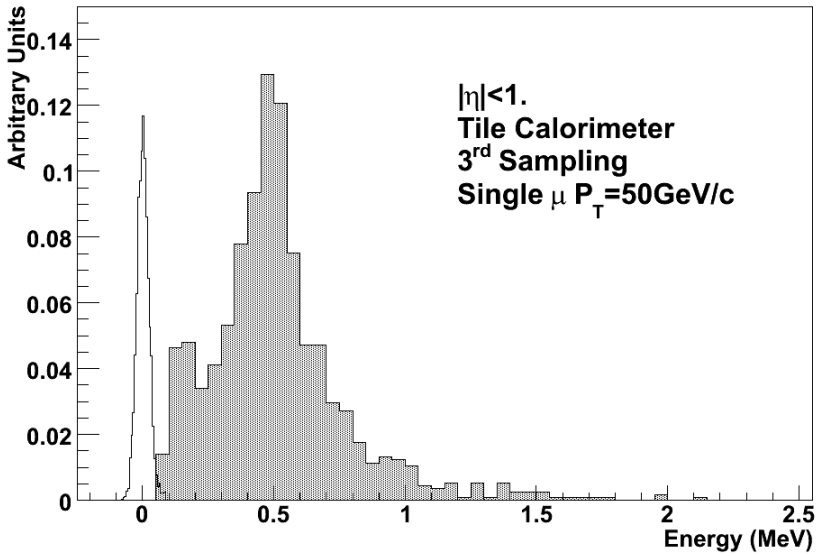

Figure 11: Comparison of signal (hatched histogram) and noise (empty histogram) distributions for the 3^{rd} sampling of the Tile Calorimeter. The most probable signal is located at $\approx 500MeV$, while the noise is peaked at $0MeV$ with a Gaussian sigma of $22MeV$.

region and measurements of the energy loss tails in the forward region. The effects of pile-up are presented in detail in Section 6.

3.4 Inert material

Although the material being sampled by the calorimeters dominates the material budget upstream of the MS, in order to achieve a reliable and accurate energy loss estimation, the energy deposition measured by the calorimeters should be corrected for the energy deposition in the inert or "dead" material of the detector. In order to perform this correction accurate knowledge of the detector material and of the muon energy loss is required. The terms inert or "dead" is used to describe the material not participating in the energy deposition measurement (ID material, cryostats, girder structure).

An accurate map of the detector material is presented[5] in Figure 12. This map was produced using the geometrical description of the ATLAS detector and the simulation package Geant 4 [6], as implemented inside ATHENA [7]. Namely, one can shoot and propagate imaginary particles, called "geantinos", inside the ATLAS detector. During their flight "geantinos" can be interrogated about their exact position, the material they traverse and its characteristics.

Figure 13 shows that the observed offset in the measured energy loss disappears when the energy deposition in the inert material is properly taken into account.

[5]The geometry tag ATLAS-DC3-02 was used.

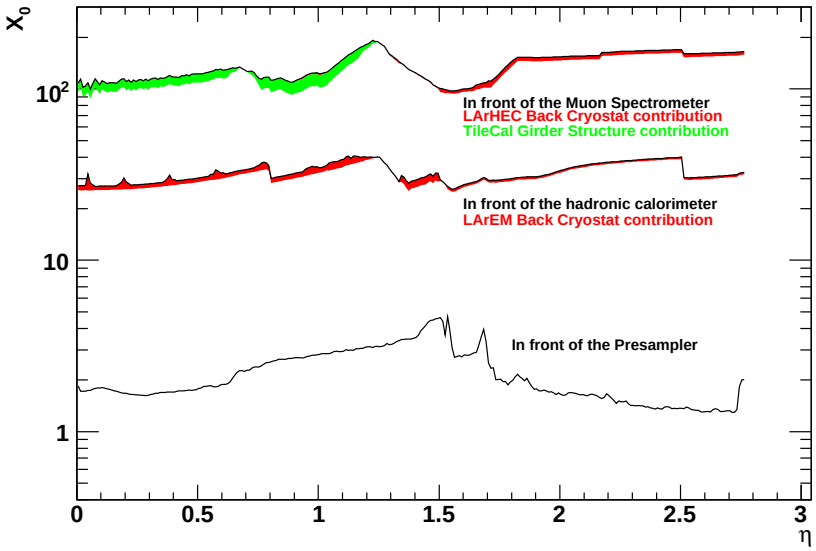

Figure 12: The material distribution in ATLAS as a function of η. The amount of material is measured in radiation lengths.

4 Study of the muon isolation criteria

The method of the "Measured" energy can only be applied to isolated muons. Its use in the case of muons which are accompanied by other particles could lead to an overestimation of their momentum. Due to the fact that muons from hadronic decays are abundant in the LHC environment, very strict criteria for "the isolation decision" have to be defined. For muons tagged as non-isolated, the *Mop* parametrization should be used.

The definition of isolated muons for this study has been performed using a *double cone strategy*. The energy collected in the inner cone is, by definition, considered as the muon energy deposition and is used for the energy loss measurement. A second coaxial cone was used for the measurement of the accompanying activity around the muon in the calorimeters and for the isolation/non-isolation decision.

In order to obtain a better understanding of the non-isolated cases, a number of $t\bar{t}$ events, with the W bosons forced to decay to muons were generated. Muons produced by hadronic decays (semi-leptonic decays of b or c quarks, e.t.c) tend to be non-isolated while those from W decays tend to be isolated. With this sample both isolated and non-isolated cases can be studied at the same time. PYTHIA [8] was used for the generation and ATHENA release 11.0.0 for the simulation, digitization and reconstruction of the $t\bar{t}$ events. The sample contained about 10^4 events.

Figure 14(a) shows an example of using only the *Mop* parametrization, as the estimation of the muon energy loss, for muons from W decays. Clearly, the negative tails corresponding to large energy losses cannot be accounted for. On the other hand, the opposite effect is

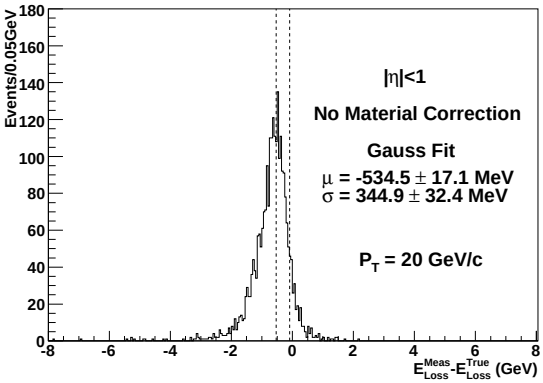

(a) Before applying the inert material correction

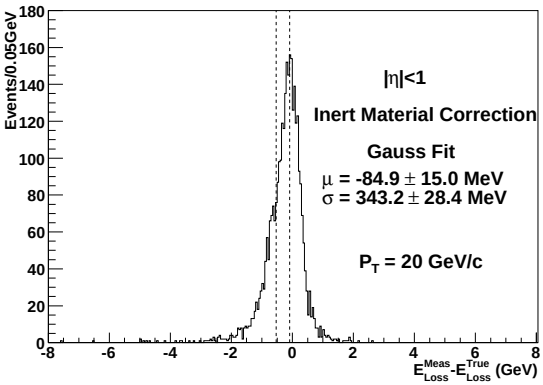

(b) After applying the inert material correction

Figure 13: Difference between the Measured and the True energy loss for single muons with $P_T = 20\,GeV/c$ and $|\eta| < 1$.

clear in Figure 14(b) when the Hybrid Meas/Mop method is used unconditionally for predominantly non-isolated muons from hadronic decays .

Two cones around each muon track were formed: The "measurement" cone, discussed in Section 3.2, and the so called "isolation" cone, formed outside the measurement cone with $R = 0.15$ for the electromagnetic calorimeter and $R = 0.30$ for the hadron calorimeters (Figure 15). The "isolation" cone could contain part of the energy accompanying the muon track if any, thus the isolation energy is defined as the difference between the energy deposition in the isolation cone and the energy deposition in the measurement cone. Different isolation cone sizes have been tried without significant influence on the results.

The energy deposition in the electromagnetic (e/m) isolation cone was found to be the most sensitive variable in order to distinguish between isolated and non-isolated muons. This can be explained mainly by the following two facts: The e/m cone is closer to the muon track than the hadronic isolation cone, meaning that a part of the energy deposition belonging to the isolation e/m cone would belong to the measurement hadronic cone.

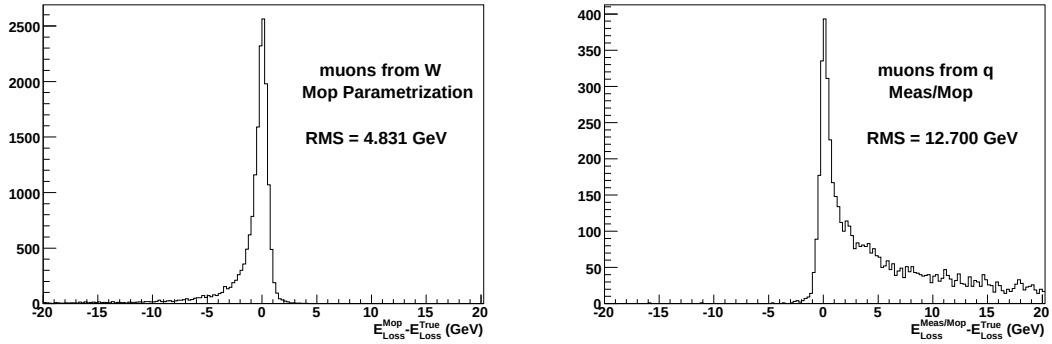

(a) (b)

Figure 14: (a) the Landau tail of the energy loss when using the *Mop* parametrization for muons from W, (b) the large tail in the energy loss when using the Hybrid Meas/Mop method without isolation criteria on predominantly non-isolated muons from hadronic decays.

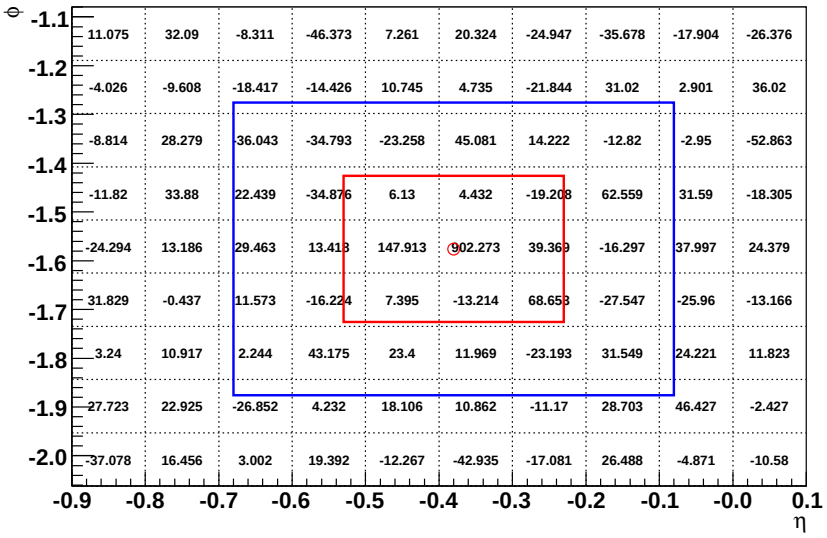

Figure 15: The Calorimeter sampling of the same event as shown in Figure 8. Besides the energy recorded in each cell (in MeV), the muon track (red circle) and the measurement area (small red square), the isolation area (large blue square) is also shown.

Furthermore, the e/m calorimeter is sensitive to both e/m clusters (photons, electrons) and the e/m part of hadronic jets, while the hadronic isolation cone is less sensitive to e/m energy depositions.

In order to define (tag) a muon as isolated, it was required that the energy deposited in the electromagnetic isolation cone was less than 2 GeV and in the hadronic one less

than $10\,GeV$. The latter had mostly the role of a safeguard rather than adding significant information to the isolation decision itself. The distributions of the isolation energies are shown in Figure 16.

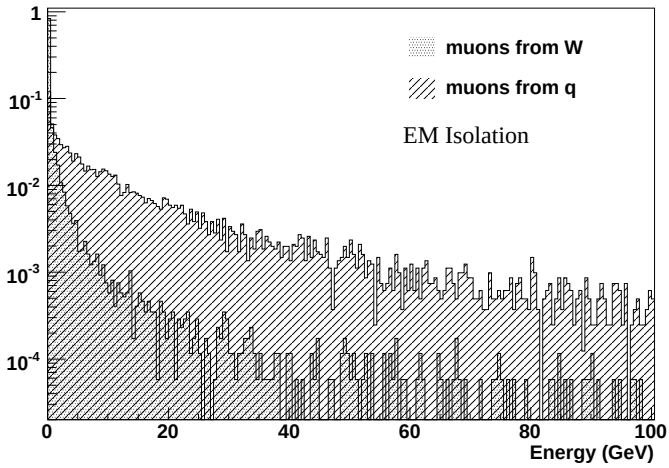

(a) Electromagnetic Calorimeter

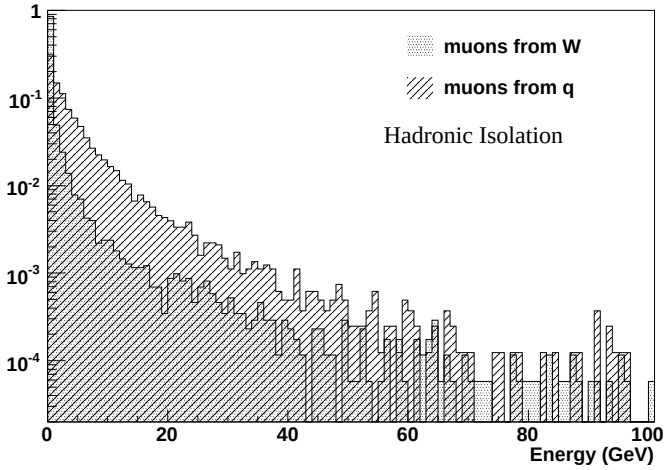

(b) Hadronic Calorimeter

Figure 16: Distribution of the isolation energy.

In Figure 17 the P_T spectra for muons from top quark decays, but separately for the leptonic W decays (a) and hadronic decays (b) are presented. For isolated muons with $P_T < 15\,GeV/c$, little gain in the energy loss estimation is obtained using the described calorimeter measurement. On the other hand, a small, but significant part of the non-isolated muons from hadronic decays with low P_T, failed to be tagged as non-isolated with the above mentioned criteria. This leads to the decision of accepting only muons with $P_T > 15\,GeV/c$ as candidates for the application of the Hybrid method. With this

additional requirement, about 83% of the muons from the W decays were tagged as isolated, whereas only 4.5% of the muons from the hadronic decays passed the isolation criteria and contaminated the isolated muon sample. At this point it is worth mentioning that the main goal of this study is not to tag the isolated muons with optimal efficiency but to maximize the improvement of the energy loss determination.

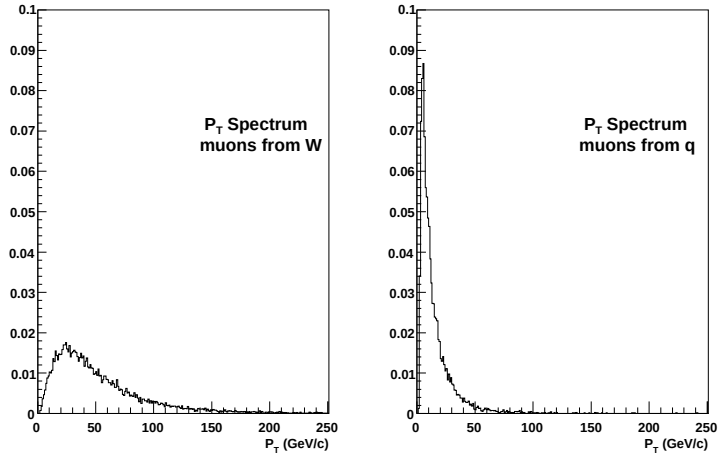

Figure 17: P_T spectrum for muons from W and hadronic decays.

The muons of the $t\bar{t}$ sample are divided into four classes: muons from W tagged as isolated, muons from W tagged as non-isolated, muons from hadronic decays tagged as isolated, muons from hadronic decays tagged as non-isolated. In Figure 18, the resolution on the energy loss obtained for each muon class is shown. It is clear that the energy loss for the majority of the muons from hadronic decays being tagged as isolated is well measured. There is, nevertheless, a tail consisting of 1.7% of the muons from hadronic decays in which the energy measurement is overestimated by more than $6\,GeV$ with respect to E_{Loss}^{True}. These muons escaped the isolation criteria already imposed, because the accompanying hadronic activity is very collimated and entirely located in the measurement cone, thus, spoiling the energy loss measurement without leaving appreciable energy traces in the isolation cone. Therefore additional information should be used in order to resolve this difficult case.

The additional information on the muon isolation can be provided by the independent ID measurement. In most cases, it is correlated with the calorimeter isolation information but in the case of collimated accompanying jets it provides the only means of discrimination for these non-isolated muons. In Figure 19 the distribution of the number of ID tracks[6] with $R < 0.2$ around the MS muon track is shown. To resolve the above mentioned cases, only muons having at most two charged tracks in the ID are tagged as isolated. In Figure 20, the resolution on the energy loss obtained for each muon class is shown after the application of this additional isolation cut.

[6]With $P_T > 1\,GeV$.

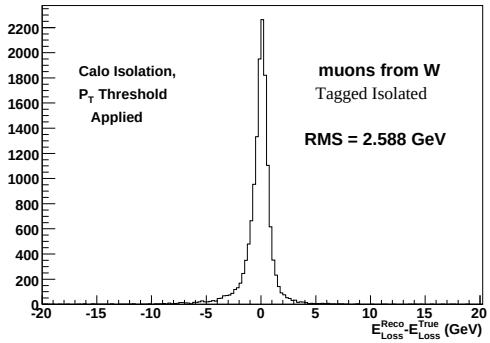

(a) Muons from W considered isolated

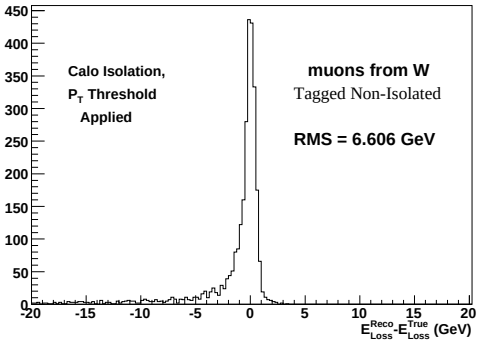

(b) Muons from W considered non-isolated

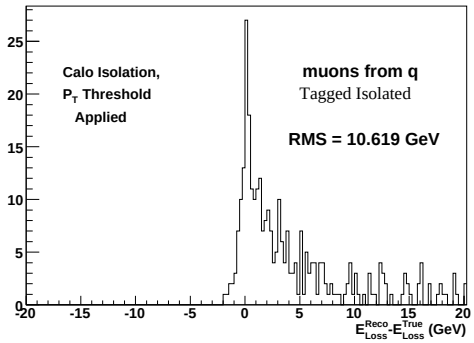

(c) Muons from hadronic decays considered isolated

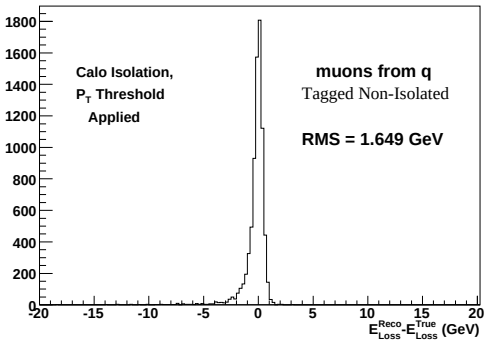

(d) Muons from hadronic decays considered non-isolated

Figure 18: Resolution on the reconstructed energy loss (Hybrid method plus isolation tagging) obtained for the four classes of events after the application of the calorimeter isolation and the P_T threshold cuts.

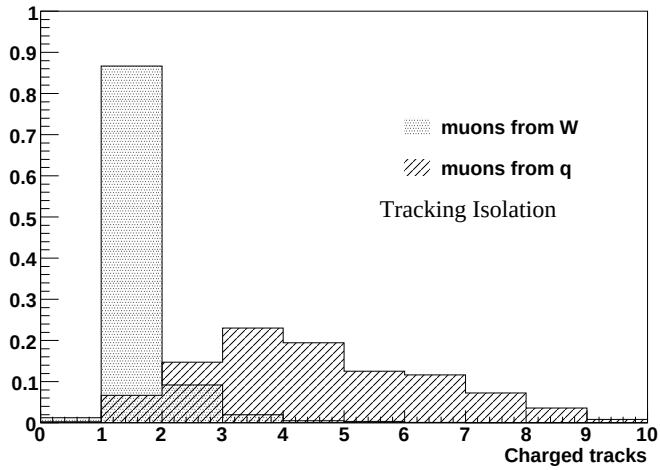

Figure 19: Distribution of the number of ID tracks with $\Delta R < 0.2$ around the MS track, after the calorimeter isolation and P_T threshold cuts are applied.

The isolation cut-flow is presented in Table 1. After all cuts are applied, only 0.15% of the muons from hadronic decays have an overestimated E_{Loss}^{Meas}, while the 80.5% of the muons from W decays are tagged as isolated and the Hybrid method is applied. In Figure 21, the fraction of single (and therefore isolated by definition) muons, where the calorimeter energy measurement is used in the Hybrid method, is presented. As expected, for P_T values above the threshold, the application of the isolation criteria has no significant effect.

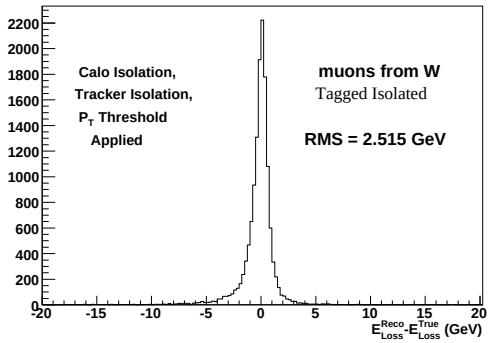

(a) Muons from W considered isolated

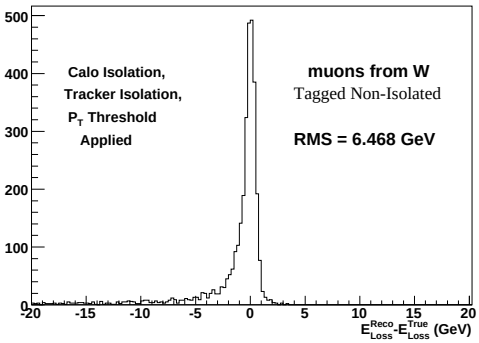

(b) Muons from W considered non-isolated

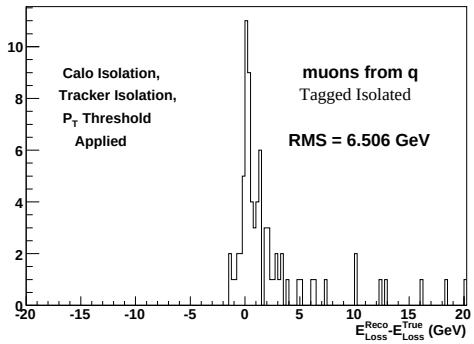

(c) Muons from hadronic decays considered isolated

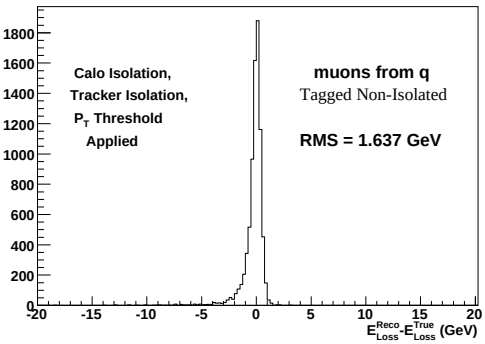

(d) Muons from hadronic decays considered non-isolated

Figure 20: Resolution on the reconstructed energy loss (Hybrid method plus isolation tagging) obtained in each of the four classes of events after all isolation cuts are applied.

At this point there was the option of extrapolating the ID tracks to the entrance of the calorimeter and then count the number of tracks around each muon. However, this approach was found to be less powerful in rejecting the non-isolated muons. The explanation is that the non-isolation is due to jet activity around the muon. Using the ID tracks expressed at the IP, is a way to identify the existence of an accompanying jet. When the muons are extrapolated to the calorimeter, the soft tracks of the jet are driven outside the track isolation cone by the magnetic field, decreasing the number of charged tracks around the muon, while the neutral particles are still inside the energy measurement cone, resulting in a reduction of the rejection power.

	Muons From W Decays (%)	Muons From Hadronic Decays (%)
No Cut	100.00	100.00
EmIso + HadIso	91.99	22.52
$P_T > 15\,GeV/c$	82.87	4.45
ID Tracks	80.45	0.964
Measured		
Within $6\,GeV$	78.55	0.815
Overestimated $> 6\,GeV$	0.64	0.148

Table 1: Cut flow for the isolation tagging.

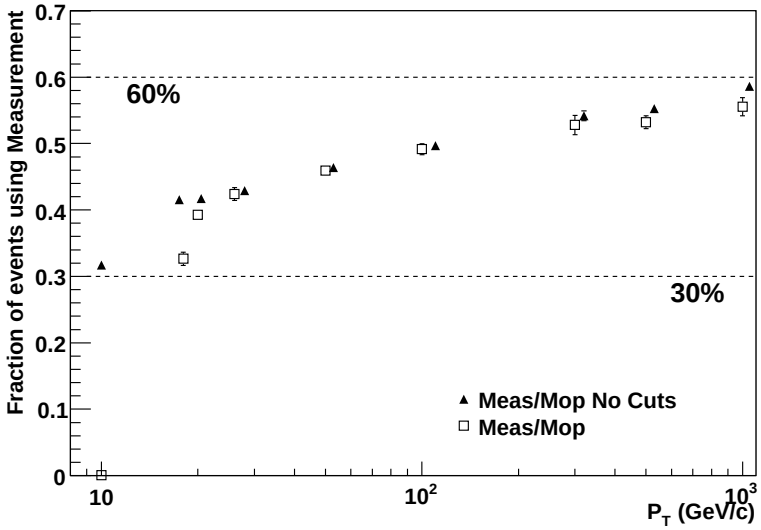

Figure 21: Effect of isolation cuts on the fraction of single muon events using the calorimeter measurement.

5 Performance evaluation of the Hybrid method

For the evaluation of the performance of the Hybrid Meas/Mop method the same set of constant P_T single muon samples as in Section 2 was used. It is reminded that, in the Hybrid method, the Measured energy was used in the cases where the muon:

- had a large energy deposition ($E_{Loss}^{Meas} > mop + 2 \cdot \sigma_{Landau}$)
- had a $p_T > 15\,GeV/c$
- was tagged as isolated

In all other cases the parametrized mop estimation was used. The procedure followed in the Hybrid Meas/Mop method is also schematically presented in Figure 22.

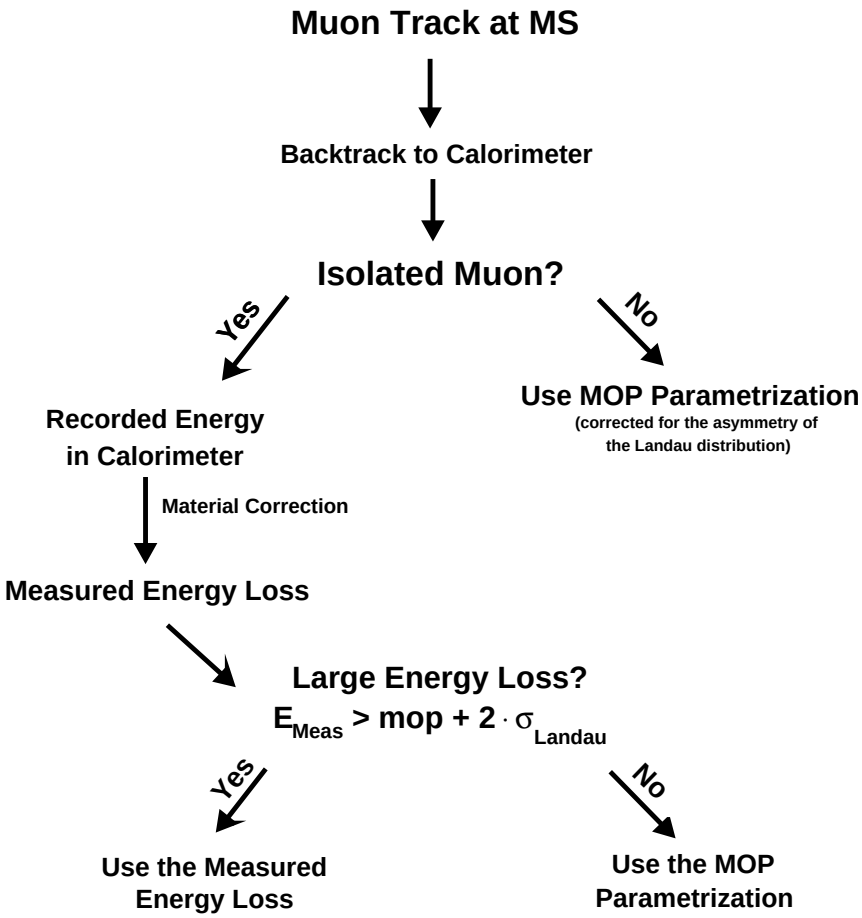

Figure 22: Flow chart of the Hybrid Meas/Mop Method.

5.1 Performance of the muon energy loss estimation

In this section, the performance of the Hybrid Meas/Mop method in the estimation of the muon energy loss upstream of the MS is discussed.

In Figure 23 the difference between the estimated and True energy loss is plotted as a function of the True energy loss. It is clear that the *Mop* parametrization cannot describe the large energy losses. For the Hybrid Meas/Mop method the shape of the scatterplot changes since the calorimeter information provides sensitivity to large energy losses.

In Figure 24 the relative energy loss resolution for the Hybrid method is presented as a function of the True energy loss. Initially, an increase in the resolution is observed when the energy loss increases. This is because in that region, the energy loss of the Hybrid method is estimated using the *Mop* parametrization. For $E_{Loss}^{True} > 7\,GeV$ the situation changes radically since the energy loss estimation is mainly determined using the measured energy loss. Thus, the relative resolution is improving with increasing E_{Loss}^{True} following the $E^{-1/2}$ law of calorimeter resolution.

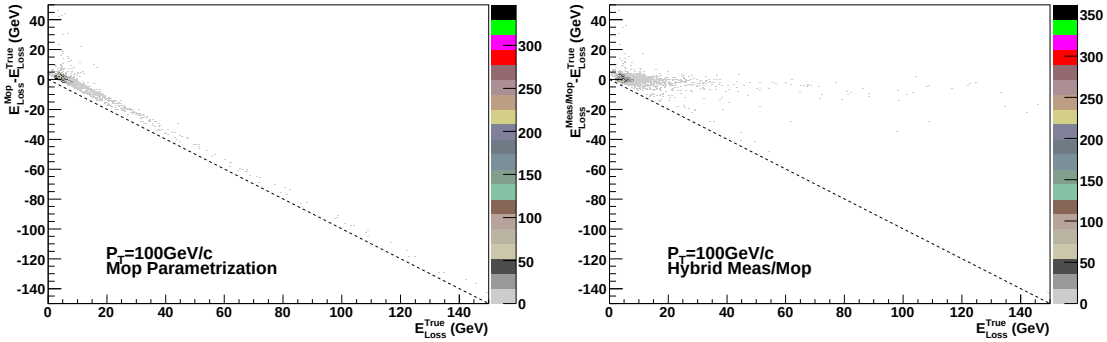

(a) Using the *Mop* parametrization. (b) Using the Hybrid method.

Figure 23: Scatterplot of the difference between the energy loss estimation and the True energy loss as a function of the True energy loss for $P_T = 100\,GeV/c$ single muons.

In Figure 25 the ratio $\sigma_{Hybrid}/\sigma_{Mop}$ of the energy loss resolutions for the Hybrid Meas/Mop method and the *Mop* parametrization respectively is shown as a function of P_T. For low P_T values the ratio is close to 1, which is expected both for the reasons explained in the previous paragraph and because of the isolation criteria imposed. However, the ratio then decreases with increasing P_T, approaching 30% at $P_T = 1000\,GeV/c$. Thus, a significant improvement in the energy loss reconstruction is gained using the Hybrid method with respect to the *Mop* parametrization.

Finally, the influence of both methods to the tails of the energy loss distribution is presented in Figure 26, where the fraction of events within $3\sigma_{Hybrid}$ is plotted for both methods. The decrease of the tails when using the Hybrid method is significant in the whole P_T range and reaches 60% for $P_T = 1000\,GeV/c$.

From the above presented results, it follows that the improvement in the muon energy loss estimation increases with increasing P_T. This was expected because the higher the muon momentum the more pronounced the energy loss tails and the induced radiation losses. However, these effects can be taken into account on an event-by-event basis only by the implementation of the Hybrid method. Furthermore, the calorimeter resolution is improving for larger energy depositions, boosting the improvement in the higher muon momenta.

5.2 Improvement of the Stand-alone muon momentum reconstruction

A necessary prerequisitive for achieving any improvement in the muon momentum resolution, via the optimum energy loss estimation, is to begin with an accurate muon reconstruction given by the standalone MS.

In Figure 27 the momentum scale is presented as function of P_T for the Hybrid Meas/Mop method and the *Mop* parametrization. The corresponding results for the muon reconstruc-

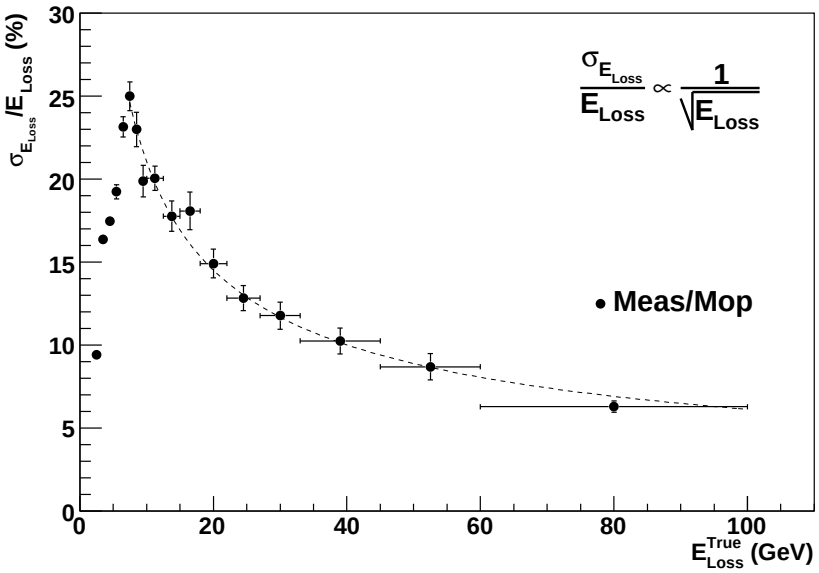

Figure 24: The relative resolution on the Hybrid energy loss estimation as a function of the True energy loss. The error on the horizontal axis indicates the bin width.

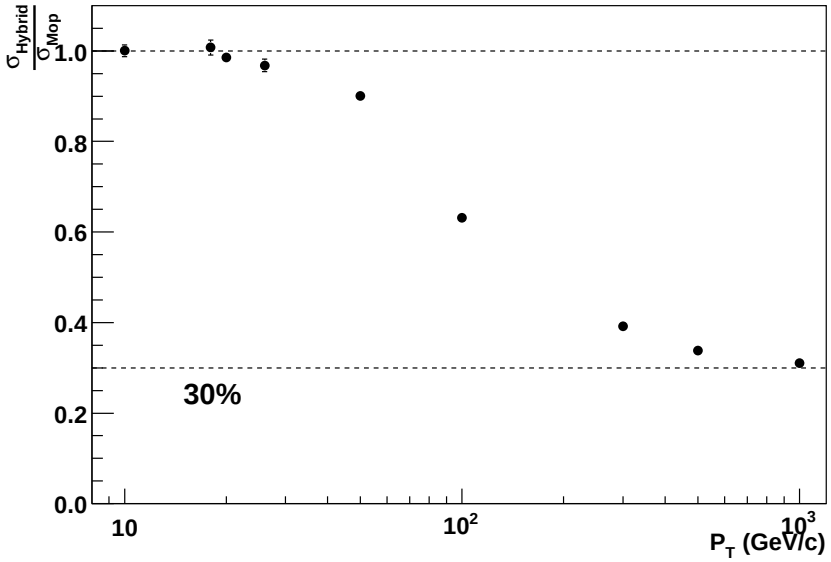

Figure 25: The ratio of the resolutions on the energy loss estimation for the Hybrid Meas/Mop method and the *Mop* parametrization.

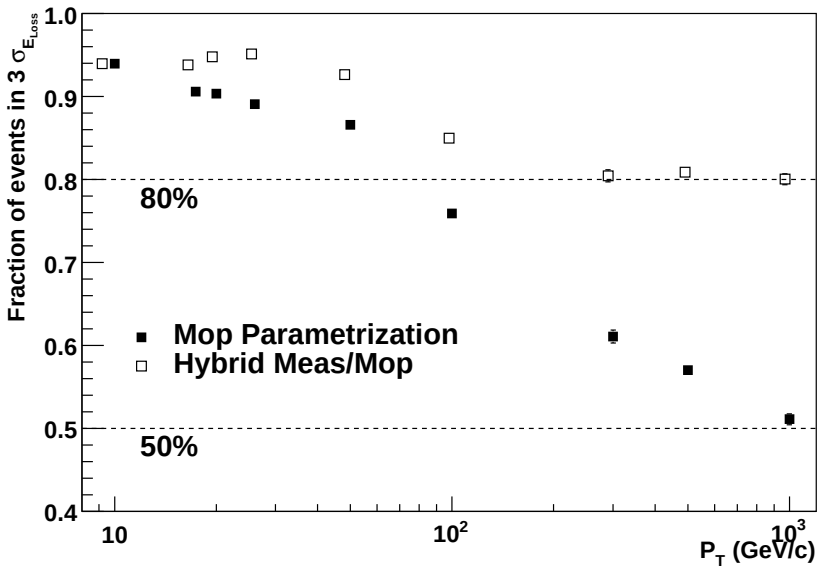

Figure 26: The fraction of events within a fixed window, $3\sigma_{Hybrid}$ of the energy loss resolution, for the parametrization and the Hybrid Meas/Mop method as a function of P_T.

tion at the MS are also presented. In the latter case, the results do not suffer from the energy loss uncertainty, since the comparison is made with the Truth information at the MS entrance.

Since both the *Mop* parametrization and the Hybrid method are very close to the momentum scale measured at the MS, it can be deduced that no systematic shift in the momentum resolution is introduced by any of the two methods.

Additionally, the Hybrid method appears to improve the resolution of the momentum measurement. This is shown in Figure 28, where the ratio of the resolutions obtained by the two methods is presented. An improvement of about 5% in most of the momentum region is observed. At low momenta, the influence of the energy loss fluctuations in the muon momentum resolution is higher but due to the small energy deposition and the isolation tagging, the benefit from the method is moderate. At high momenta, the benefit from the use of the Hybrid method is larger, but so is the uncertainty originating from the MS reconstruction. The latter reduces the impact of the energy loss fluctuations on the momentum resolution.

The improvement in the energy loss estimation has also some impact on the tails of the momentum distribution. In Figure 29, the fraction of muons having a measured momentum within $3\sigma_{Hybrid}$ of the relative momentum resolution is plotted. As explained above, the largest improvement with the Hybrid method is observed in the P_T region between 30 and 100 GeV/c.

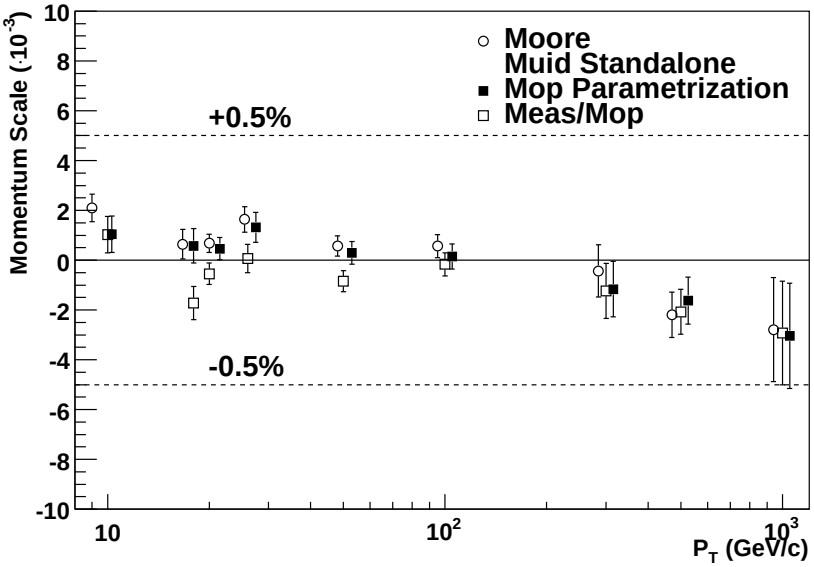

Figure 27: Momentum scale for Stand-alone muon reconstruction as a function of the P_T. The corresponding results of muon reconstruction at the MS (Moore) are also presented.

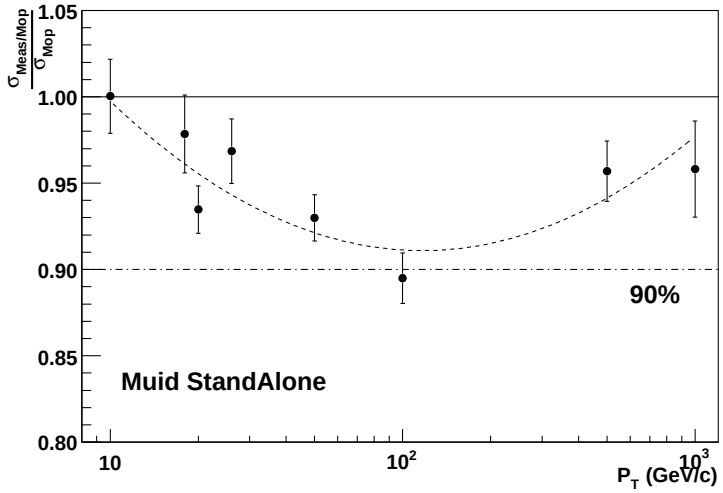

Figure 28: Ratio of the momentum resolutions of stand-alone muon reconstruction using the Hybrid method to the *Mop* parametrization method. The parabolic line is a guide to the eye.

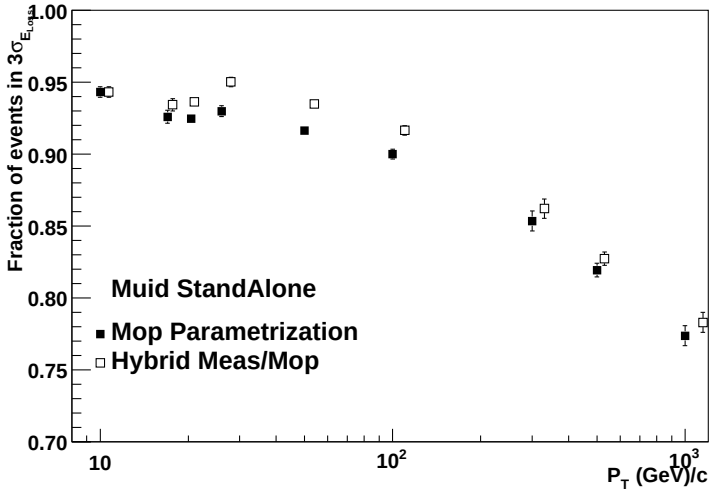

Figure 29: Fraction of muons within $3\sigma_{Hybrid}$ of the relative momentum resolution for the Hybrid method and for the *Mop* parametrization.

5.3 Improvement of the Combined muon momentum reconstruction

As it has been already explained (Section 1), in the combined muon reconstruction the MS and the ID measurements are combined to achieve the best estimation for the muon track parameters. The energy loss upstream the MS makes the connection between the measurements of the two subsystems. However, the influence of the energy loss fluctuations in the combined momentum resolution is directly correlated with the weight of the MS measurement contribution on the combined MS/ID track. Thus, it is expected that the benefit of using the Hybrid method with respect to the *Mop* parametrization will be maximal in the momentum range between 80 and 500 GeV/c. Besides, it should be noted that the accurate estimation of the energy loss upstream the MS is an important factor for the correct matching between the MS and ID tracks.

In Figure 30 the momentum scale -using the Hybrid method- is compared for the stand-alone and for the combined reconstruction. In both cases the result is consistent with zero in the whole momentum region from 10 GeV/c up to 1000 GeV/c.

In Figure 31 the ratio of the combined reconstruction resolutions obtained by the two methods is presented. As expected, the improvement at low momenta and very high momenta is marginal, but all of the 10% improvement of the stand-alone reconstruction at $P_T = 100\,GeV/c$ is propagated to the combined reconstruction.

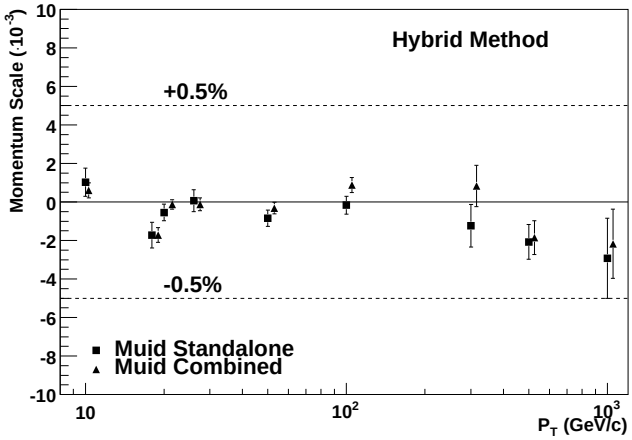

Figure 30: Momentum scale for Stand-alone and Combined muon reconstruction, using the Hybrid method, as a function of the P_T.

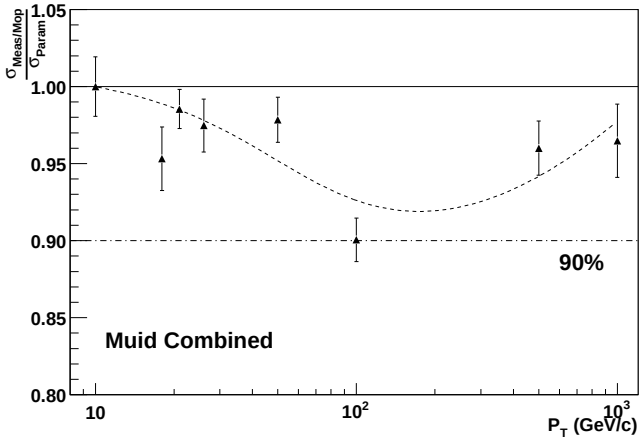

Figure 31: Ratio of the momentum resolutions of Combined muon reconstruction using the Hybrid method to the *Mop* parametrization method. The dashed curve is a guide to the eye.

6 Pile-up and cavern background studies

In order to investigate how the energy deposition measurement is influenced by the induced noise due to pile-up events and cavern background conditions, the study was repeated for single muons[7] of $P_T = 100 GeV/c$ with different pile-up and cavern background conditions. The study shows that no significant deterioration of the energy estimation is introduced with higher luminosities up to five times the initial low luminosity value or with higher cavern backgrounds up to five times the nominal one. It must be stated, right from the beginning, that the following results are valid only for muons with $|\eta| < 2$. For technical reasons, fixed in subsequent software releases, the reconstruction of muons with higher $|\eta|$ has been problematic.

Figure 32(a) shows that the effect of the pile-up in the mean value of the distribution is more pronounced in the measured part of the energy loss estimation. The effect however, is very much reduced when the Hybrid method is used. Nevertheless, even this small effect can be corrected for by subtracting the Mean Noise contribution, calculated for the specific luminosity conditions.

Beside the effect on the mean value (energy scale), the different noise conditions also affect the resolution of the measurement. Taking a worse case scenario, where the noise threshold is unchanged with respect to the no pile-up case, the spread of the energy measurement distribution is increased by 20%. The resulting final energy calculation, however, worsens only by 8% (Figure 32(b)). This can also be corrected for by adjusting the cell noise thresholds to the running conditions.

Finally, in Figure 32(c) it is shown that the non-Gaussian tails of the energy loss estimations do not increase using the different luminosity conditions of the study.

7 Conclusions

An improved and updated parametrization of the muon energy loss upstream of the MS, accompanied by asymmetric errors accounting for the asymmetry of the Landau energy loss distribution, is described and implemented in the official ATLAS software. At the same time, a correction for the shift caused by the convolution of the Gaussian distribution of the momentum measurement and the asymmetric nature of the Landau energy loss is also introduced.

A method for the estimation of the muon energy loss using as input the calorimeter information is presented. This energy loss measurement is incorporated to a Hybrid method combining both the calorimeter measurement and the *Mop* parametrization. For isolated muons with measured energy loss consistent with the mop energy, the latter is used for their energy loss estimation, while for isolated muons with a large measured energy deposition, the measured energy loss is used. In the case of non-isolated muon, the corrected *Mop* energy loss parametrization is used.

[7] Simulated and digitized with release 10.0.1, reconstructed with release 10.4.0.

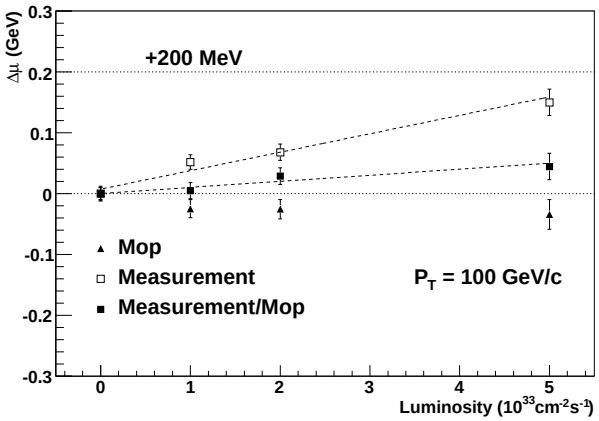

(a) The Gaussian mean of the E_{Loss} resolution expressed as difference from the zero luminosity result.

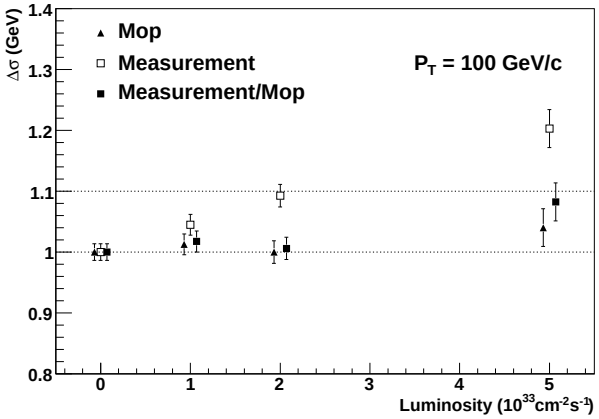

(b) The Gaussian σ of the E_{Loss} resolution normalized to the zero luminosity result.

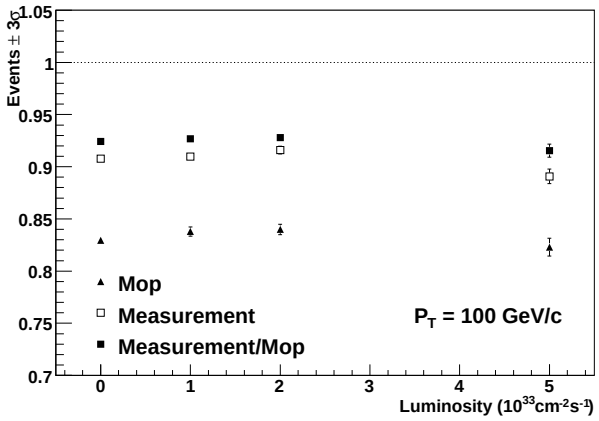

(c) Fraction of events within a fixed window (3σ of the E_{Loss} resolution).

Figure 32: Effect of pile-up on the estimation of the energy loss as a function of luminosity.

The use of this Hybrid method significantly improves the resolution of the muon energy loss estimation and reduces the non-Gaussian tails. A significant fraction of this improvement is propagated to the stand-alone and combined muon momentum measurements offering an average 5% improvement in the relative momentum resolution, reaching 10% for $P_T = 100\, GeV/c$.

8 Acknwoledgements

We would like to thank Stephane Willocq, Dan Levin and Kyle Cranmer for fruitful discussions.

The project is co-funded by the European Social Fund and National Resources - (EPEAEK II) PYTHAGORAS II.

References

[1] ATLAS Collaboration, "ATLAS Detector and Physics Performance Technical Design Report Vol I", CERN-LHCC-99-14 (1999).

[2] W. M. Yao *et al.* [Particle Data Group], J. Phys. G **33** (2006) 1.

[3] J.Shank *et al.*, ATLAS Internal Note, ATL-SOFT-2003-007 (2003);
T. Lagouri *et al.*, IEEE Trans. Nucl. Sci. **51**, 3030 (2004).
https://uimon.cern.ch/twiki/bin/view/Atlas/MooreMuid

[4] M. Virchaux *et al.*, ATLAS Internal Note, ATL-MUON-97-198 (1997).
http://atlas-samusog.web.cern.ch/atlas-samusog/muonboy/Muonboy.htm

[5] Atlas Collaboration, "ATLAS Calorimeter Performance", CERN-LHCC-96-40 (1996).

[6] J. Allison *et al.*, IEEE Trans. Nucl. Sci. **53** (2006) 270.
S. Agostinelli *et al.* [GEANT4 Collaboration], Nucl. Instrum. Meth. A **506** (2003) 250.
(http://geant4.web.cern.ch/geant4/)

[7] ATHENA manual, http://atlas.web.cern.ch/Atlas/GROUPS/SOFTWARE/
OO/architecture/General/Tech.Doc/Manual/ 2.0.0-DRAFT/AthenaDeveloperGuide.pdf

[8] T. Sjostrand, S. Mrenna and P. Skands, JHEP **0605** (2006) 026.
arXiv:hep-ph/0603175
(http://www.thep.lu.se/~torbjorn/Pythia.html)

[9] S. Menke, **Noise suppression methods**, Jets/$\not\!\!E_T$/τ Session, ATLAS Physics Workshop, Rome 2005.
http://indico.cern.ch/conferenceDisplay.py?confId=a044738

Appendices

A Data samples

In the following table (Table A-1) the constant P_T single muon samples used to assess the performance of the muon energy loss estimation methods are summarized. The samples were simulated and digitized using ATHENA release 11.0.41[8] and reconstructed with ATHENA release 12.0.1.

Data Sample	Events
csc11.007211.singlepart_mu10.digit.RDO.v11000401	4600
csc11.007216.singlepart_mu18.digit.RDO.v11000401	4000
csc11.007218.singlepart_mu20.digit.RDO.v11004202	10000
csc11.007222.singlepart_mu26.digit.RDO.v11000401	5100
csc11.007231.singlepart_mu50.digit.RDO.v11000401	9800
csc11.007233.singlepart_mu100.digit.RDO.v11000401	8500
mc11.004934.mu_pt300.digit.RDO.v11000401	3000
csc11.007235.singlepart_mu500.digit.RDO.v11000401	7000
csc11.007236.singlepart_mu1000.digit.RDO.v11000401	3900

Table A-1: Summary of the sinle muon data samples used in this study.

B The systematic shift induced by the use of *Mop* parametrization in the momentum estimation

B.1 Understanding the induced shift

As already explained, the distribution of the energy loss of muons is asymmetric in nature with a long tail towards the large energy losses.

One way to proceed with the energy loss correction is to use the Most Probable Value (mop) of the muon energy loss. This is a characteristic quantity of the energy loss distribution and the muon is more likely to loose this amount of energy before reaching the MS.

However, the convolution of the symmetric resolution of the MS and the asymmetric resolution of the energy loss induces a systematic shift to the momentum resolution at the IP. In order to estimate the systematic effect, a toy Monte-Carlo has been set up. Muons of $P = 100\,GeV$ where produced and suffered energy loss in a random fashion, following a Landau distribution with $mop = 3\,GeV$ and $\sigma_{Landau} = 0.4\,GeV$[9]. The momentum left

[8]Except for the $P_T = 20\,GeV/c$ sample where release 11.0.42 was used.

[9]This is typical energy loss distribution for muons with $P = 100\,GeV/c$ in ATLAS.

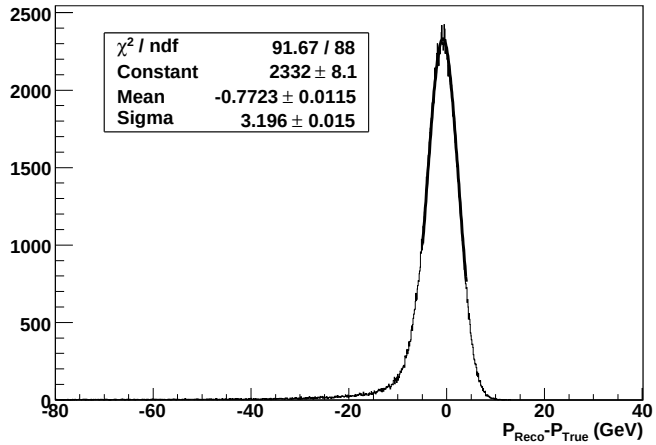

Figure B-1: The resolution of the muon momentum reconstruction for $\alpha = 3\%$. The momentum is systematically underestimated by $770 MeV/c$.

after the loss was smeared by a Gaussian resolution $\sigma_P = \alpha \cdot P$[10], which represented the MS measurement error, to produce the "measured" momentum.

Using this "measured" momentum we reconstructed the muon energy at the IP by always adding to it the nominal mop of the energy loss, i.e. $3\,GeV$. The difference between the final reconstructed momentum and the muon momentum for $\alpha = 3\%$ is shown in Figure B-1. The reconstructed momentum is systematically lower than the initial one, namely a systematic shift has been introduced.

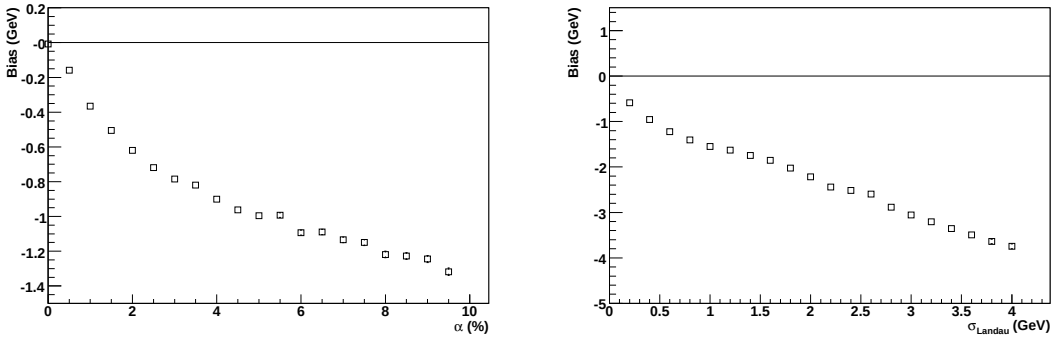

(a) (b)

Figure B-2: The dependence of the momentum shift (a) on $\sigma_P = \alpha \cdot P$ and (b) on σ_{Landau}.

To study this effect further, the above mentioned parameters were kept constant and the momentum resolution was left free to vary. Figure B-2(a) shows that the introduced shift increases with increasing measurement resolution.

[10]The resolution is considered constant and independent of the measured energy

Another way to study the effect is to vary σ_{Landau}, the sigma of the Landau distribution, keeping constant the measurement resolution. The evolution of the shift as a function of the σ_{Landau} is shown in Figure B-2(b).

B.2 Correcting for the introduced shift

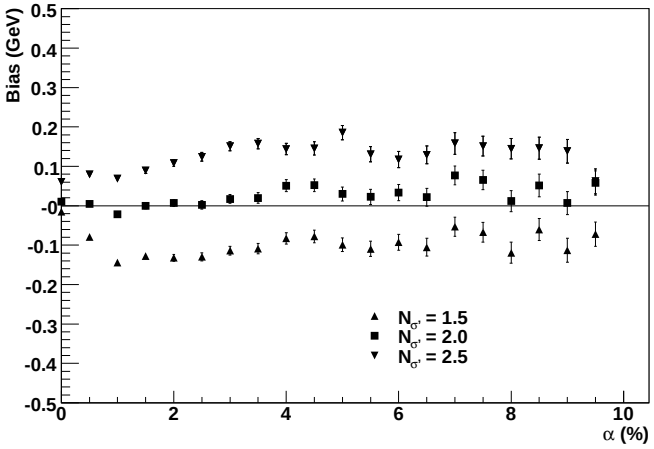

Figure B-3: The shift as a function of the resolution for different values of $N_{\sigma'}$.

From the above discussion is obvious that the use of the *Mop* parametrization "out of the box" is not the proper way to correct for the energy loss, since it introduces the above mentioned shift.

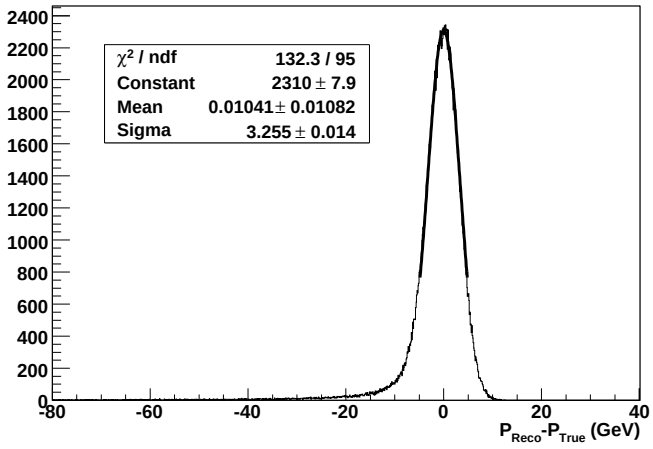

Figure B-4: The distribution of Figure B-1 after the correction is applied. No systematic shift is observed.

This effect can be accounted for by calculating and using a weighted mean of the Landau distribution in a symmetrical region around the peak. In this way, the energy loss correction is perfomed taking into account the asymmetry of the energy loss distribution, which is the main reason for the shift.

The weighted mean is calculated in the region $[mop - N_{\sigma'} \cdot \sigma', mop + N_{\sigma'} \cdot \sigma']$ where $\sigma' = \sigma_P \oplus \sigma_{Landau}$[11]. In order to determine the value of $N_{\sigma'}$, in Figure B-3 the induced shift as a function of σ_P is shown for three different values of $N_{\sigma'}$. The value $N_{\sigma'} = 2$ clearly offers the best cancellation of the introduced shift. Figure B-4 shows the correction applied on the muons of Figure B-1.

Finally, the effect of the corrected appproach is presented as a function of σ_P, Figure B-5(a), and σ_{Landau}, Figure B-5(b). The latter plot justifies the usage of σ' instead of using σ_P alone.

The above results were applied to the official ATLAS Monte-Carlo. The results for single muons of $P_T = 100\,GeV/c$ were presented in Section 2 (Figure 6).

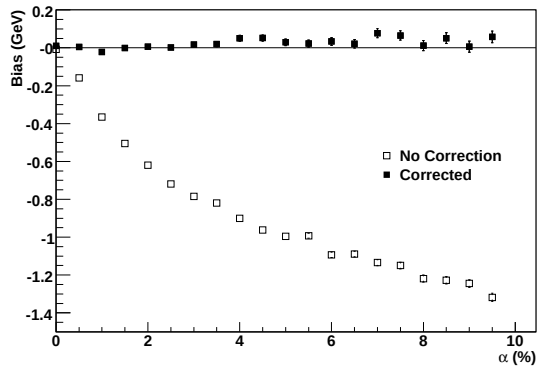

(a) The evolution of the shift as a function of σ_P.

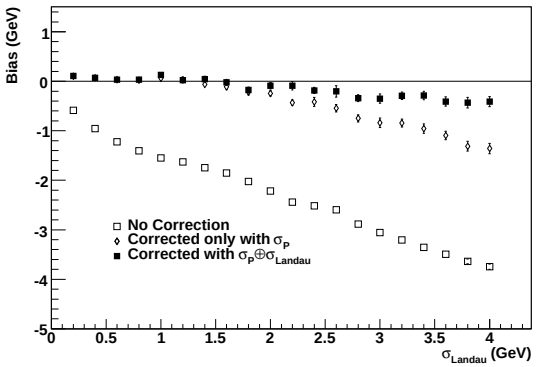

(b) The evolution of the shift as a function of σ_{Landau}.

Figure B-5: The induced shift before and after the suggested correction. Momentum reconstruction is roughly unbiased after the correction.

C Combining the energy loss measurement with the *Mop* parametrization

Since the energy resolution of the calorimeters roughly scales as $\frac{\sigma_E}{E} = \frac{a}{\sqrt{E}}$, it is clear that the smaller the energy deposition of the muon, the less accurate the calorimeter measurement.

As explained in tha main text, in the introduced "Hybrid method", the *Mop* parametrization of the muon energy loss is used together with the measured energy deposition in a

[11]The symbol $\oplus$ denotes addition in quadrature.

complementary way.

The only free parameter in the Hybrid method is the point of the energy loss distribution where the transition from the *Mop* parametrization to the measured energy and vice versa will be made. The shift in the momentum estimation as a function of the MS resolution for different transition values $E_{transition} = mop + N_\sigma \cdot \sigma_{Landau}$ is presented in Figure C-1. It can be seen that if the value $N_\sigma = 2$ is used, the resulting momentum distribution has no shift.

This plot justifies the choice of Section 3.1 to use the measurement only when the measured energy loss is greater than $mop + 2 \cdot \sigma_{Landau}$ and the *Mop* parametrization for the rest of the cases.

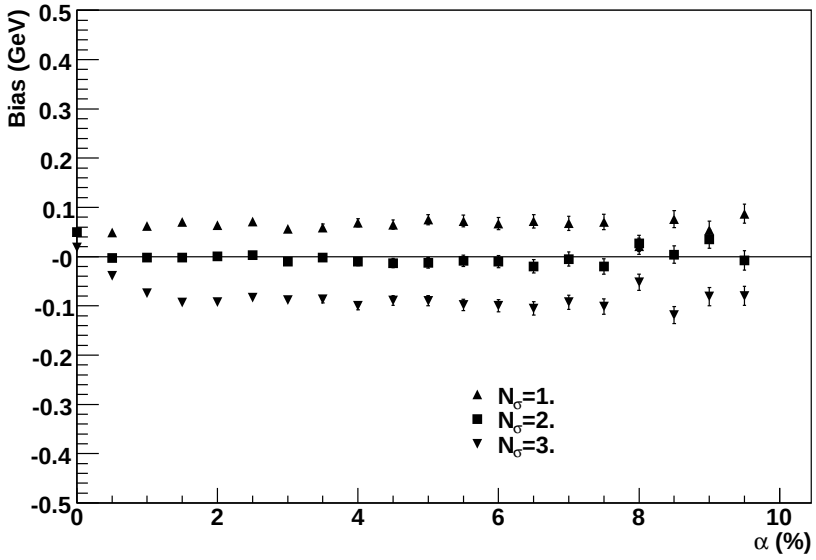

Figure C-1: The induced shift as a function of the resolution for different N_σ.

D Noise levels of the calorimeter cells

In this Appendix the characteristics of the noise distribution are presented for zero luminosity and the low initial luminosity ($10^{33} cm^{-2} s^{-1}$).

In order to extract the mean value and the sigma of the noise in the case of zero luminosity, where only electronic noise is present, a Gaussian fit to the noise distribution of each sampling was performed.

For $10^{33} cm^{-2} s^{-1}$, where both electronic and pile-up noise are present, a fit with the sum of two independent Gaussian functions was performed to the noise distribution of each sample. In Tables D-1 and D-2, the mean and the sigma of the broader of the two Gaussian functions is given. Note that the narrow one is compatible with the results for zero luminosity.

In Figure D-1 the estimated distribution of the electronic noise as a function of the η of the cell is given for the three different ATLAS calorimeters. One should note that only the region with $|\eta| < 2.7$ is interesting from the MS point of view, since this is the region where the MS provides coverage. However, the following results refer to the full calorimeter coverage.

	Zero Luminosity	Low Luminosity
Tile		
1	0.42	-0.54
2	-0.30	-0.63
3	-1.88	-1.60
ITC	-0.03	-0.82
LArHEC		
1	0.16	124.2
2	-0.31	38.9
3	-1.88	16.7
LArEM		
Presampler	0.53	9.9
1	0.50	13.1
2	0.52	28.6
3	0.54	0.75

Table D-1: Mean value of the noise in MeV.

	Zero Luminosity	Low Luminosity
Tile		
1	25.5	26.0
2	25.5	25.6
3	23.5	23.4
ITC	12.2	12.8
LArHEC		
1	161.3	358.0
2	227.0	329.5
3	297.7	412.9
LArEM		
Presampler	54.1	128.9
1	13.3	28.1
2	30.5	115.8
3	23.9	24.9

Table D-2: Sigma of the noise in MeV.

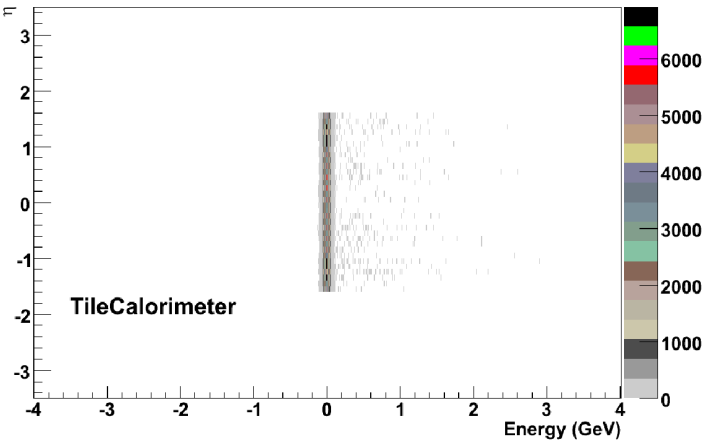

(a) Tile Calorimeter

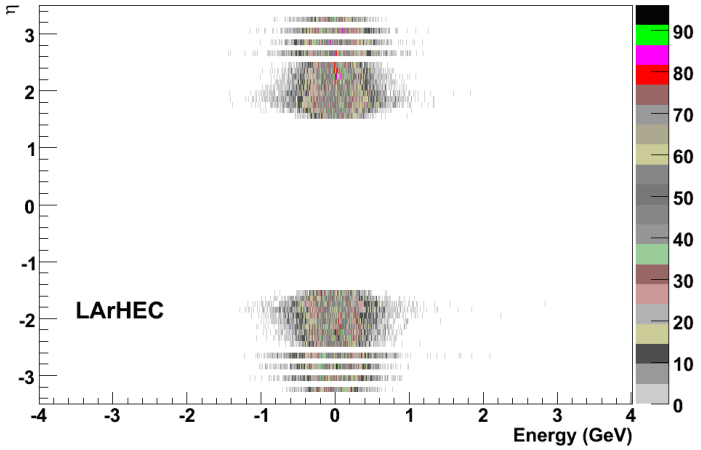

(b) LAr Hadronic Calorimeter

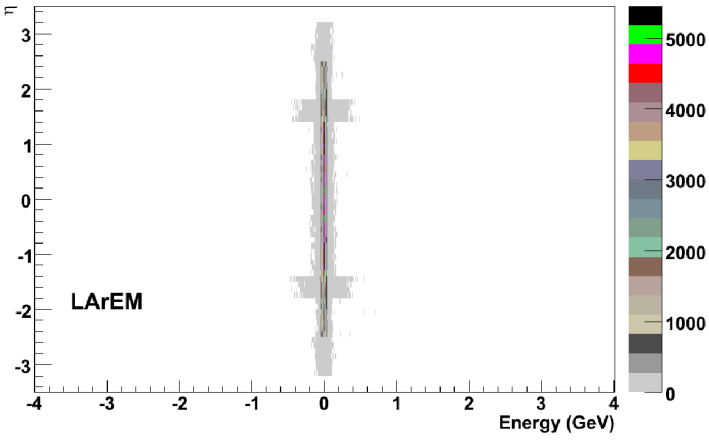

(c) LAr Electromagnetic Calorimeter

Figure D-1: Electronic noise distribution in ATLAS calorimeters as a function of η.

E Forward calorimeter correction

In Section 3.1 the implemented noise suppression scheme[12] is given. It has been demonstrated [9] that these asymmetric noise suppresion schemes lead to a systematic underestimation of the energy measurement with the introduced shift being more pronounced when the expected signal is of comparable magnitude with the noise threshold. In the presented study, this remark is relevant mainly for the LArHEC calorimeter.

Without pile-up, the expected σ_{Noise} in LArHEC is $O(200MeV)$, resulting in a noise threshold of $O(800MeV)$[13], while the expected muon signal for the first LArHEC sampling can be roughly estimated to $O(400MeV)$[14]. The comparison of the expected signal and the corresponding noise threshold leads to the conclusion that the mop energy loss is well below the noise threshold, i.e. it is not possible to use the LArHEC to measure energy depositions around the mop. However, it is still possible to measure the Landau tail of the muon energy loss. This is true since the muon energy loss in different calorimeter samplings is roughly uncorrelated[15] (Figure E-1). Thus, the Landau tail is formed mainly by a large energy deposition in one sampling.

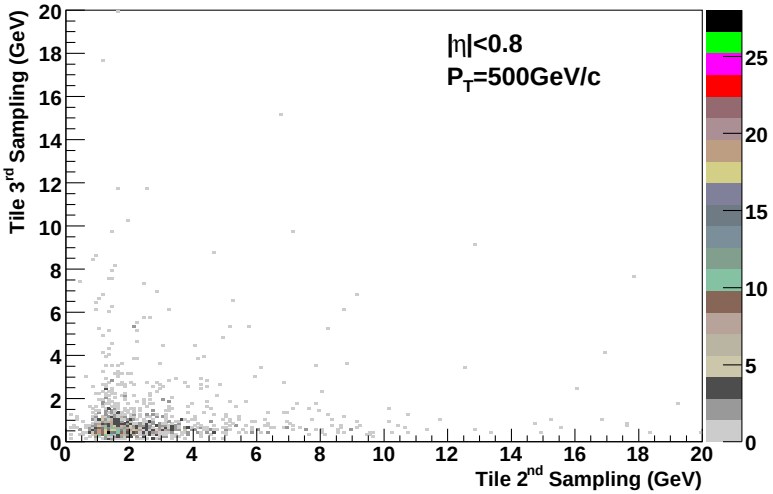

Figure E-1: Scatterplot of the energy deposition in the 2^{nd} and 3^{rd} Tile Calorimeter samplings, for single muons with $P_T = 500\ GeV/c$ and $|\eta| < 0.8$. The linear correlation coefficient is $r = 0.05$, thus the energy deposition in the different samplings is uncorrelated.

Therefore, the situation where a large energy deposition is measured in one LArHEC sampling and no signal above threshold is observed in the other samplings is quite usual.

[12] $E_{Cell} > 4 \cdot \sigma_{Noise}$

[13] In the presence of pile - up the situation is worse, especially for the first LArHEC sampling.

[14] $E_{expected}$ = (Expected energy loss upstream of the MS)·(Fraction of material upstream of the MS present in LArHEC)·(Fraction of LArHEC material in its 1^{st} sampling)$= 3\,GeV \cdot 0.95 \cdot 0.14 \approx 400\,MeV$

[15] Assuming that the energy loss in one sampling is small compared to the momentum of the muon.

If zero energy loss is attributed in those samplings, a bias is introduced resulting to a systematic underestimation of the muon energy loss in the forward region. However, the nature of muon energy loss permits the correction of this effect. When no signal above threshold is seen for a muon in one sampling, it can be rather reasonably argued that it had a minimum ionizing behaviour. Using this assumption, the expected energy loss at the particular sampling can be estimated rather accurately.

The effect of this correction is shown in Figure E-2 for single muons in the forward region with $P_T = 20\,GeV/c$.

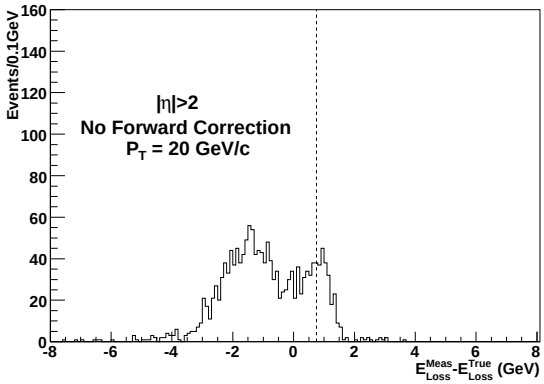

(a) Without forward calorimeter correction

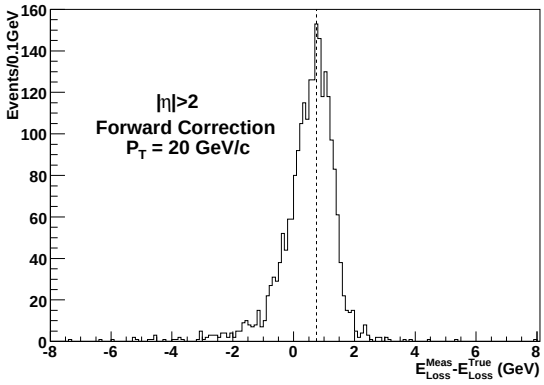

(b) With forward calorimeter correction

Figure E-2: The difference between the Measured energy loss and the True energy loss, before and after applying the forward calorimeter correction.